Food Hydrocolloids 172 (2026) 111908

Contents lists available at ScienceDirect

Food Hydrocolloids

journal homepage: www.elsevier.com/locate/foodhyd

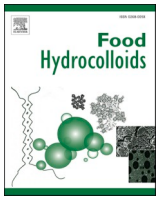

Lubrication and delubrication behaviour of micron-sized whey protein microgels

Qi Wang [a,b,c], Siavash Soltanahmadi [c], Jianshe Chen [a,b,**], Anwesha Sarkar [c,*]

[a] Laboratory of Food Oral Processing, School of Food Science and Biotechnology, Zhejiang Gongshang University, Hangzhou, Zhejiang, 310018, China
[b] Zhejiang-UK Joint Laboratory of Food Sensory Science, Zhejiang Gongshang University, Hangzhou, 310018, China
[c] Food Colloids and Processing Group, School of Food Science and Nutrition, University of Leeds, Leeds, LS2 9JT, UK

ARTICLE INFO

Keywords:
Oral tribology
Biomimetic tongue
Friction
Viscosity
Particle
Roughness

ABSTRACT

This study aims to understand the tribological properties of whey protein microgels (WPM) by varying their sizes in the micron-scale and deformability. To decipher the lubrication mechanisms of WPM dispersions (3–48 vol %), we explored two tribological systems *i.e.* conventional smooth substrate and novel biomimetic tongue-like surfaces. We fabricated relatively *hard* WPM (G' ≈ 350 kPa) of three distinct sizes ($D_{4,3}$ ≈ 1–50 μm) and *soft* WPM (G' ≈ 85 kPa, $D_{4,3}$ ≈ 50 μm) using water-in-oil emulsion templating. On smooth surfaces, dispersions of *soft* WPM delivered good lubrication in boundary and mixed regimes across the studied volume fractions (3–48 vol %), which was attributed to deformation-induced entrapment of WPM and the resulting surface separation. In contrast, *hard* WPM appeared to be entrapped between the contacting surfaces when their size was comparable to the theoretically derived film thickness (*e.g.* 1 μm). The incorporation of 1 μm *hard* WPM caused delubrication, which can be attributed to increased proportion of surface asperities disrupting the aqueous lubrication. In a simulated tongue-palate interface (biomimetic tongue), microgel participation through the collision between WPM and the tongue-like papillated structure was found to be largely delubricating irrespective of size in the micron-scale, which we postulate can be caused by jamming of microgel particles and/or even deformation of the papillae-like features by WPM. Our findings demonstrate that *hard*, micron-sized WPM exhibit delubrication when relatively soft tongue-like surfaces are employed. These insights can inspire development of food products where an interplay between size and deformability of semi-solid particles is key to modulate mouthfeel.

1. Introduction

Microgels are submicron-to micron-sized, gel-like particles composed of cross-linked polymers that trap solvent within their network. For food, these particles can be formed from single or mixed biopolymers using methods based on physical and chemical gelation (Farjami & Madadlou, 2017; Murray, 2019; Nicolai, 2016; Nicolai & Durand, 2013) or the controlled fragmentation of the parent gels. Owing to their inherent biocompatibility and low toxicity compared to synthetic alternatives (Akgonullu et al., 2023), biopolymer-based microgels, such as those derived from natural polysaccharides and proteins, have attracted extensive research interest for food technological applications, including use as Pickering stabilizers (Sarkar & Dickinson, 2020; Tenorio-Garcia et al., 2024; You et al., 2024), drug delivery agents (Sivakumaran et al., 2011), and food-grade 3D printing inks (Highley et al., 2019). Notably, their functionality also extends to rheological modification and lubrication-enhancement under conditions relevant to oral processing (Andablo-Reyes et al., 2019; Gabriele et al., 2010; Garrec & Norton, 2013; Kew et al., 2023; Sarkar et al., 2017; Soltanahmadi et al., 2022).

Numerous efforts have been made to explore the possibility of whey protein in particular to form whey protein microgels (WPM) for lubrication applications, employing fabrication techniques that primarily consist of controlled protein network growth ("bottom-up" approach) and parent gel fragmentation ("top-down" approach) (Murray, 2019). Mechanically breaking down the parent gel has been widely recognized as facile route to yield submicron-sized microgels with a relatively narrow size distribution. It is widely reported in literature that WPM exhibited superior lubrication as compared to native whey protein solutions, largely attributed to a combination of surface

* Corresponding author.
** Corresponding author. Zhejiang-UK Joint Laboratory of Food Sensory Science, Zhejiang Gongshang University, Hangzhou, 310018, China.
E-mail addresses: jschen@zjgsu.edu.cn (J. Chen), A.Sarkar@leeds.ac.uk (A. Sarkar).

https://doi.org/10.1016/j.foodhyd.2025.111908
Received 29 May 2025; Received in revised form 26 July 2025; Accepted 25 August 2025
Available online 1 September 2025

adsorption-aqueous lubrication, viscosity-facilitated surface separation and a soft ball-bearing mechanism in tribological contacts (Kew et al., 2023; Sarkar et al., 2017). A key limitation of this method is the poor control over elasticity, as the rigid parent gel often fails to pass smoothly through confined homogenization channels, increasing dispersion heterogeneity. Moreover, achieving particle sizes in the tens of microns is challenging due to the narrow window of size variation possible with the fixed gaps in the jet homogenization process (Akgonullu et al., 2024).

Alternatively, emulsion templating methods, including both water-in-water (W/W) and water-in-oil (W/O) approaches, offer a robust bottom-up strategy for fabricating micron-sized spherical WPM with controllable size and modulus from protein solutions *via* chemical cross-linking or heat setting (Beldengrün et al., 2018; Chu et al., 2022; Çakır & Foegeding, 2011). Micron-sized WPM prepared *via* W/W emulsion templating method (*i.e.*, protein-polysaccharide segregative phase separation) have been shown to effectively reduce friction on steel-3M surgery tape contacts, even outperforming saliva (Chu, et al., 2022, 2024), but cause delubrication when tested against compliant neoprene interfaces compared to the polysaccharide matrixes (xanthan gum), highlighting that surface mechanics critically dictate particle-mediated lubrication (Chojnicka-Paszun et al., 2014). However, the final protein concentration of microgel produced *via* W/W templating may differ from the stock protein solution due to the excluded volume effects in the protein-rich phase. This also, makes it hard to determine the actual elastic modulus of microgels (Chu et al., 2024).

To date, the lubrication mechanisms of the micron-sized microgels have not been systematically elucidated *via* experimental methods, with respect to size and modulus. Of more importance, studies are far more limited in tribology of micron-sized WPM especially within tribological conditions relevant to oral processing such as using human tongue-like textured surfaces. The human tongue is a unique muscular organ, with its anterior two-thirds covered with various papillae (*i.e.*, filiform, fungiform, circumvallate and foliate papillae), contributing to an overall surface roughness in the order of hundreds of microns (Andablo-Reyes et al., 2020; Kullaa et al., 1985; Wang et al., 2021). Although the topographic structure of the tongue is well poised for feeding and speech (Moayedi, et al., 2018, 2021), its impact on oral lubrication and texture perception, particularly in the presence of particulate lubricants such as WPM remains poorly understood. Wang et al. (2022) highlighted a potential correlation between the tongue surface roughness and *in situ* friction coefficients using natural plant fiber dispersions, where higher tongue roughness resulted in increased friction.

While previous studies have explored the effects of particle size and volume fraction on the tribological performance of sub-micron-sized WPM dispersions, these particles are produced with relatively low protein concentrations (≤15 wt %), rendering them much softer than the tribopair material (typically PDMS or glass). This disparity may not accurately represent the range of food materials present in real tongue-palate contacts, where harder particles are also commonly present (de Wijk & Prinz, 2005; Imai et al., 1999; Liu et al., 2016; Soltanahmadi et al., 2023). The main reason for wider investigation of soft microgels perhaps is associated with their preferable deformability and thus, facilitates better entrapment within the contact region, without eliciting undesired sensory perception (Shewan et al., 2020). However, overly soft microgel can show limited ability in supporting loads, leading to increased boundary friction, a critical factor in applications such as tongue-hard palate contacts (Gabriele et al., 2010; Garrec et al., 2013). Collectively, there is a clear knowledge gap in understanding the tribological performance of micron-sized microgels in the literature with limited insights on how deformability and size can affect their lubrication. In addition, to date there is no study that has examined the behaviour of such micron-sized microgels in biomimetic tongue-like surface that has texture, softness and wettability similar to a real human tongue.

The aim of this study was therefore to elucidate the tribological mechanisms of micron-sized whey protein microgel (WPM) dispersions, by examining how particle size, deformability, as well as volume fraction affect frictional behavior. To this end, we fabricated relatively *hard* WPM (25 wt % protein content, storage modulus G' ≈ 350 kPa) of three distinct sizes ($D_{4,3}$ ≈ 1, 10, 50 μm) and *soft* WPM variant (15 wt % protein content, G' ≈ 85 kPa, $D_{4,3}$ ≈ 50 μm) using water-in-oil emulsion templating. Particle size and microstructure of WPM were characterized by light scattering and confocal microscopy. We further investigated the influence of tribopair surface micro-topography (smooth *vs.* tongue-mimetic) on these dispersions, with volume fractions of WPM ranging from 3 to 48 vol %, using two tribometry setups, namely, a ball-on-smooth disc and a ball-on-biomimetic tongue, providing a comprehensive assessment of system parameters under physiologically relevant contact conditions. Overall, this study aims to provide critical insights into the relevance of the particle size, volume fraction, and deformability of micron-sized microgels in real oral processing conditions for the first time.

2. Materials and methods

2.1. Materials

Whey protein isolate powder (WPI, protein content ≥90 %) was kindly supplied by Fonterra Limited (Auckland, New Zealand). Sodium caseinate powder (bovine origin) was purchased from Sigma-Aldrich, New Zealand and Span® 80 was purchased from Sigma-Aldrich, UK. Polyglycerol polyricinoleate (PGPR) was kindly donated by Palsgaard (Denmark). Sunflower oil was obtained from a local supermarket (Tesco Express, Leeds, UK). Milli-Q water with a resistivity of 18 MΩ cm was produced using a Milli-Q apparatus (Millipore Corp., Bedford, MA, USA). A 20 mM phosphate buffer was prepared by dissolving sodium phosphate monobasic monohydrate and sodium phosphate dibasic anhydrous (Thermo Fisher Scientific, Loughborough, UK) in Milli-Q water, and was used both to dissolve WPI powder and as a dispersing medium for preparing WPM dispersions. Sodium azide (0.02 wt%) (Sigma-Aldrich, Gillingham, UK) was employed as a preservative. Ecoflex™ 00–30 (Smooth-On, USA) was purchased from Amazon (UK).

2.2. Methods

2.2.1. Preparation of WPM dispersions

The WPM dispersions were prepared using a bottom-up emulsion templating method, originally described by Sağlam et al. (2011), with minor modifications. A schematic overview of the preparation procedure is shown in Fig. 1 A. This method mainly involves three steps: (i) the formation of a coarse W/O emulsion, (ii) heat-induced gelation of whey protein droplets, and (iii) separation and washing of the gelled WPM. A whey protein isolate (WPI) solution (15 wt % or 25 wt %) was prepared by dissolving WPI powder in 20 mM phosphate buffer at pH 7.0 for 2 h and stored at 4 °C overnight to ensure complete solubilization. Sunflower oil was mixed with 2.5 wt % PGPR as a hydrophobic emulsifier under magnetic stirring for 2 h. The particle size of WPM was largely governed by the droplet size of water-in-oil (W/O) emulsions. Therefore, to achieve a desired particle size, the WPI solution was slowly introduced into the oil phase while mixing with either a high-speed mixer (Ultra-Turrax T 25, IKA Werke, Germany) or an overhead mini mixer (MINISTAR 40 control, IKA Werke, Germany). For instance, to produce W/O emulsion droplets of approximately 1 μm ($D_{4,3}$), the WPI solution was added to the oil under continuous mixing at 10,000 rpm for 6.5 min using the high-speed mixer. For WPM of ~10 μm, the primary emulsion was stirred at 900 rpm for 8 min. For 50 μm particles, irrespective of the WPI content, the stirring was carried out at 500 rpm for 3 min using an overhead mixer. Accordingly, based on their WPI contact and particle size, WPM produced from 25 wt % WPI solution are denoted as "*hard* WPM-1 μm", "*hard* WPM-10 μm", and "*hard* WPM-50 μm", while the soft variant (15 wt % WPI content) is designated as "*soft* WPM-50 μm", enabling investigation of size and deformability effects (Fig. 1B).

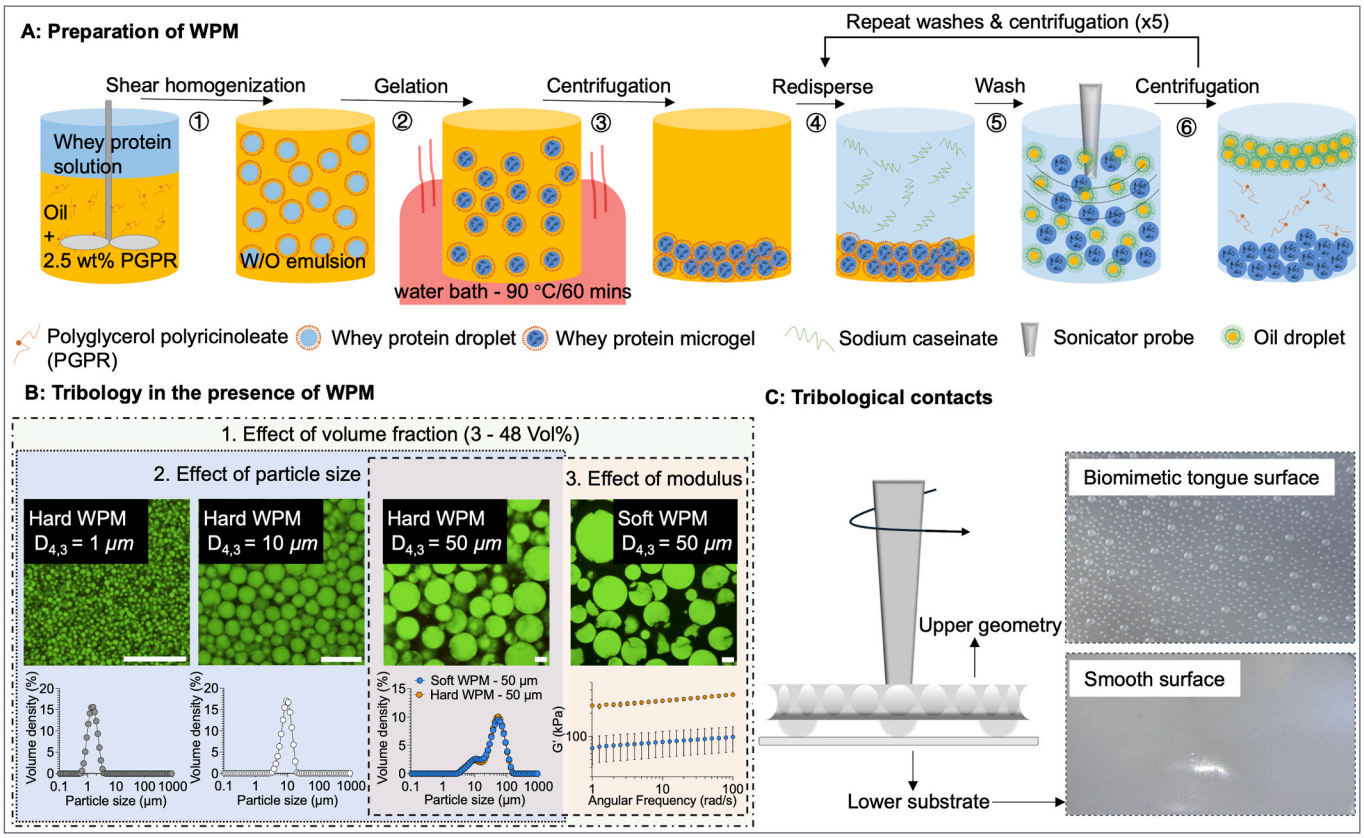

Fig. 1. Schematic illustration (A) of the fabrication method for micron-sized whey protein microgels (WPM). Confocal laser scanning microscopy (CLSM) images (B) of WPM (top) of various sizes and moduli and mean particle size distributions of WPM obtained *via* static light scattering (bottom). (C) Schematic illustration of two tribological contacts: ball-on-smooth surface and ball-on-biomimetic tongue surface. Scale bars in A and B are 20 μm. In A and B, red color represents oil phase stained by Nile Red and green represents protein stained by Fast Green. (For interpretation of the references to color in this figure legend, the reader is referred to the Web version of this article.)

The ratio of the water phase to the oil phase in the primary emulsion was 3:7 (w/w). The W/O emulsion was then carefully transferred into several 50 mL centrifuge tubes and heated in a water bath at 90 °C for 1 h with gentle agitation to thermally crosslink and gel the water droplet *via* hydrogen bonding, hydrophobic interactions, and disulfide bonds to form the spherical microgels. The heat-set WPM were separated from the emulsion using a high-speed centrifuge (Avanti J-30I, Beckman Coulter, USA) to remove majority of the oil (continuous phase). The resulting pellet, consisting primarily of WPM was carefully collected and re-dispersed in a 4 wt % sodium caseinate solution at a weight ratio of 1:3 w/w. Excess oil on the WPM surface was removed by forming an oil-in-water (O/W) emulsion *via* shear homogenization and sonication (750 W, VCX750, Sonics & Materials, INC, USA). The emulsified oil droplets were subsequently removed through repeated centrifugation and washing steps (Fig. 1A). This centrifugation and washing procedure with sodium caseinate solution was repeated three times, followed by two more washes with 20 mM phosphate buffer to ensure that most of the oil was removed from the WPM's surfaces. Accurately quantifying the effective volume fraction of microgels is always challenging because they may release aqueous phase during shear or centrifugation. Here, we distinguish apparent differences in particle concentration by defining the centrifuged pellet as 100 vol %, and lower volume fractions of microgels (3–48 vol %, see Eq. (1)) were obtained by redispersing the pellets (WPM) in 20 mM PBS buffer. The resultant dispersions were then kept in fridge at 4 °C and were sonicated with 20 % of its full power (150 W) for 5 min before rheological, tribological as well as particle size characterization.

Volume fraction of WPM dispersions was calculated using Eq. (1):

$$vol\,\% = \frac{Vol_{WMP}}{Vol_{WMP} + Vol_{Buffer}} = \frac{mWPM/\rho WPM}{mWPM/\rho WPM + mBuffer/\rho Buffer}, \quad (1)$$

where, m_{WPM} is the weight of the pellet (mainly consist of WPM), ρ_{WPM} is the density of WPM (assumed to be equivalent to that of WPI solution: 1.05 g/mL, González-Tello et al. (2009)), m_{buffer} and ρ_{buffer} is the weight and density (1.00 g/mL) of the buffer.

2.2.2. Flow behavior and apparent viscosity of WPM dispersions

Rheological properties of WPM dispersions (3–48 vol %) were measured using a modular compact rheometer (MCR-302, Anton Paar, Austria) at 25 °C. A parallel-plate (PP 50, diameter: 50 mm, operating gap: 1000 μm) geometry was used for all measurements. Approximately, 1950 μL of each sample was carefully transferred onto the bottom plate while avoiding the introduction of any air bubbles. The samples were initially measured at a pre-shear step at $\gamma = 1\ s^{-1}$ for 60 s to reach a steady state, followed by logarithmic ramping of shear rate from 0.1 to 1000 s^{-1}. At each shear rate, a 30 s interval was allowed to ensure stress stability. Means were calculated from three independent measurements.

2.2.3. Small deformation rheology

Viscoelastic properties of macroscopic whey protein hydrogels (15 or 25 wt % WPI in buffer) were investigated separately by oscillatory shear rheology using a modular compact rheometer (MCR-302, Anton Paar, Austria) equipped with a cone-and-plate geometry (CP50-1, diameter 50 mm, cone angle 1°). The initial setup initialized a 0.208 mm gap between the cone and plate, and silicon oil was applied around the cone to prevent sample evaporation. Storage (G′) and viscous (G″) moduli were measured by applying a temperature ramp to characterize gelation

behavior and then, frequency sweeps were performed on the gelled protein samples. In details, samples were heated from 25 °C to 90 °C at a rate of 0.08 °C/s under a constant strain of 0.1 % at 1 Hz and held at 90 °C for 60 min. The temperature was then lowered to 37 °C at the same rate, and a frequency sweep from 1 Hz to 100 Hz at a 0.1 % strain was performed. Means were calculated from three independent measurements.

2.2.4. Particle size distribution

Particle size distribution of WPM was determined at room temperature (~25 °C) using a laser diffraction particle size analyzer (Mastersizer 3000, Malvern Instruments, Worcestershire, UK). WPM dispersions, both before and after tribological measurement, were carefully collected, gently stirred, and diluted by adding particles into the aqueous measurement cuvette until the instrument reached an optimal obscuration rate of approximately 10 %. To resolve the particle size distribution from scattering data, a refractive index of 1.33 for the aqueous phase and 1.53 for the protein phase (WPM) was assumed. The analysis was set for regular spherical particles, and each sample was measured in quintuplicate. The mean particle size of WPM was reported as the volume mean diameter ($D_{4,3}$). The particle size distribution of each sample was measured at least three times.

2.2.5. Confocal Laser Scanning Microscopy (CLSM)

The microstructure of 12 vol % dispersions of WPM, both before and after exposure to tribological shear was studied using a Zeiss LSM 880 inverted confocal microscope (Carl Zeiss MicroImaging GmbH, Jena, Germany) equipped with a 40 × oil immersion lens. Nile Red solution (1 mg/mL in dimethyl sulfoxide, Sigma-Aldrich) was used to stain sunflower oil to a final concentration of 0.02 mg/mL, while a Fast Green solution (1 mg/mL in Milli-Q water) was used to stain WPM to a final concentration of 0.1 mg/mL. Approximately 150 μL of WPM dispersion, both before and after tribological test, was mixed with Fast Green and Nile Red for 15 min and was pipetted into a concave slide. Nile Red was excited at a wavelength of 488 nm, and Fast Green at 633 nm. The emission filters were set at 555–620 nm for Nile Red and 660–710 nm for Fast Green.

2.2.6. Soft tribology

Tribological measurements of WPM dispersions at different volume fractions (3–48 vol %) and buffer at pH 7 were performed using a tribometer based on MCR-302 rheometer (Anton Paar, Austria) using a three glass hemispheres-on-disc setup (T-PID/44, MCR Tribology Cell). As we schematically illustrated in Fig. 1C, the lower substrates employed were a smooth elastomer surface and a previously described biomimetic tongue, exhibiting a static water contact angle of ~60°, designed to emulate the mechanical and surface physicochemical characteristics of a human tongue. Both substrates were fabricated *via* soft lithography (Andablo-Reyes et al., 2020; Hu et al., 2020; Soltanahmadi, et al., 2022, 2023). The fabrication of the biomimetic tongue has been detailed elsewhere (Andablo-Reyes et al., 2020; Soltanahmadi et al., 2022). Briefly, a mixture of elastomer (Ecoflex™ 00–30 containing 0.5 wt % Span 80 and 1 wt % SLO-JOTM™ Platinum Silicone Cure Retarder) was homogeneously mixed and degassed using a mixing and degassing apparatus (ARE-250, Intertronics, Kidlington, UK). Subsequently, 7.10 g of the degassed elastomer mixture was carefully weighed and transferred onto the 3D-printed negative master mould, allowing it to spread and cover the mould surface, which had been pre-coated with a thin layer of a release agent (Ease Release™ 200, Smooth-On, USA). The entire setup was then placed in a vacuum oven for 30 min to control sample thickness and remove any trapped air bubbles within the papillae-simulating indentations. Following overnight curing at room temperature, the solidified elastomer substrate was carefully peeled off the mould and sonicated in pure isopropanol, 5 wt % detergent solution, and Milli-Q water for 5 min each. Smooth surfaces were fabricated using similar procedure, except that a stretched Parafilm was placed over the negative mould to create a flat surface before transferring the elastomer.

The elastomer substrate was secured onto the rheometer's bottom Peltier plate using a stainless-steel chamber assembly, which includes a 50 mm diameter disc sized to match the substrate dimensions and a top annular fixer that fastens the substrate's periphery *via* threaded tightening. A total normal force of 1.0 N was then applied, compressing three glass hemispheres against the substrate. Consequently, each glass hemisphere experienced a normal force of ~ 0.33 N. Tests were conducted at room temperature (~25 °C) under pure sliding in a unidirectional rotary contact. The sliding speeds were increased logarithmically from 5×10^{-6} m s^{-1} to 2 m s^{-1}. This MCR tribology cell allows the calculation of the friction coefficient based on the torque (τ), applied normal force (F) and the radial distance between the center of the glass hemisphere and the center of the bottom plate (r), as in Eq. (2):

$$\mu = \frac{\tau}{Fr} . \quad (2)$$

Results were presented as the mean ± standard deviation from one measurement on three separate substrates for each dispersion.

2.2.7. Statistical analyses

Statistical analyses were performed using one-way ANOVA after confirming normality (Shapiro-Wilk test) and homogeneity of variance (Levene's test); when these assumptions were violated, the nonparametric Kruskal-Wallis test was applied. Differences were considered significant at $p < 0.05$.

3. Results and discussion

3.1. Confocal microscopy and size of WPM

For illustration purpose, the CLSM images of WPM with particle size of approximately 1 μm ($D_{4,3}$) obtained at different fabrication stages are shown in Supporting Fig. S1, showing the effective oil removal stage to create the WPM. The CLSM images of all the WPM dispersions following final washing and centrifugation steps, are shown in Fig. 2. The *hard* WPM made from 25 wt % WPI solution are shown in Fig. 2A–C, with Fig. 2A depicting particle size of 1 μm and Fig. 2B and C shows particle size of 10 μm and 50 μm, respectively. To investigate the influence of particle deformability on lubrication, relatively *soft* WPM with a diameter of 50 μm were also fabricated using the method described ahead. Unlike their *hard* counterparts, these *soft* WPM failed to maintain a spherical morphology in the entirety of the size distribution range, as shown in Fig. 2D, instead, some breakdown of particles could be observed. Such damage is attributed to the mechanical agitation involved in the washing process, during which some of the *soft* WPM might have broken up when subjected to mechanical shear and sonication.

The size distribution of WPM after removal of the oil was determined *via* light scattering, as shown in Fig. 2A_3-D_3 and $D_{4,3}$ is detailed in Table 1. All the dispersions exhibit polydispersity in size. WPM with average diameter of 1 μm and 10 μm showed a monomodal, whereas the *soft* and *hard* WPM with an average diameter of 50 μm showed a bimodal particle size distribution.

3.2. Elastic modulus of whey protein gels

The particle size, deformability, and volume fraction of WPM are widely recognized as key factors influencing the rheological properties of WPM dispersions (Andablo-Reyes et al., 2019; Chu et al., 2024; Sarkar et al., 2017). The shear modulus (G′) of WPM was assumed to be similar to that of the parent gel prepared using 15 wt % or 25 wt % WPI, which was evaluated using oscillatory shear rheology (temperature ramp and frequency sweeps, Supporting Fig. S2). The G′ of WPI gels at 25 wt % protein content was approximately 350 kPa. The G′ taken from after heat treatment for 30 min is about 12 kPa, which aligns well with the

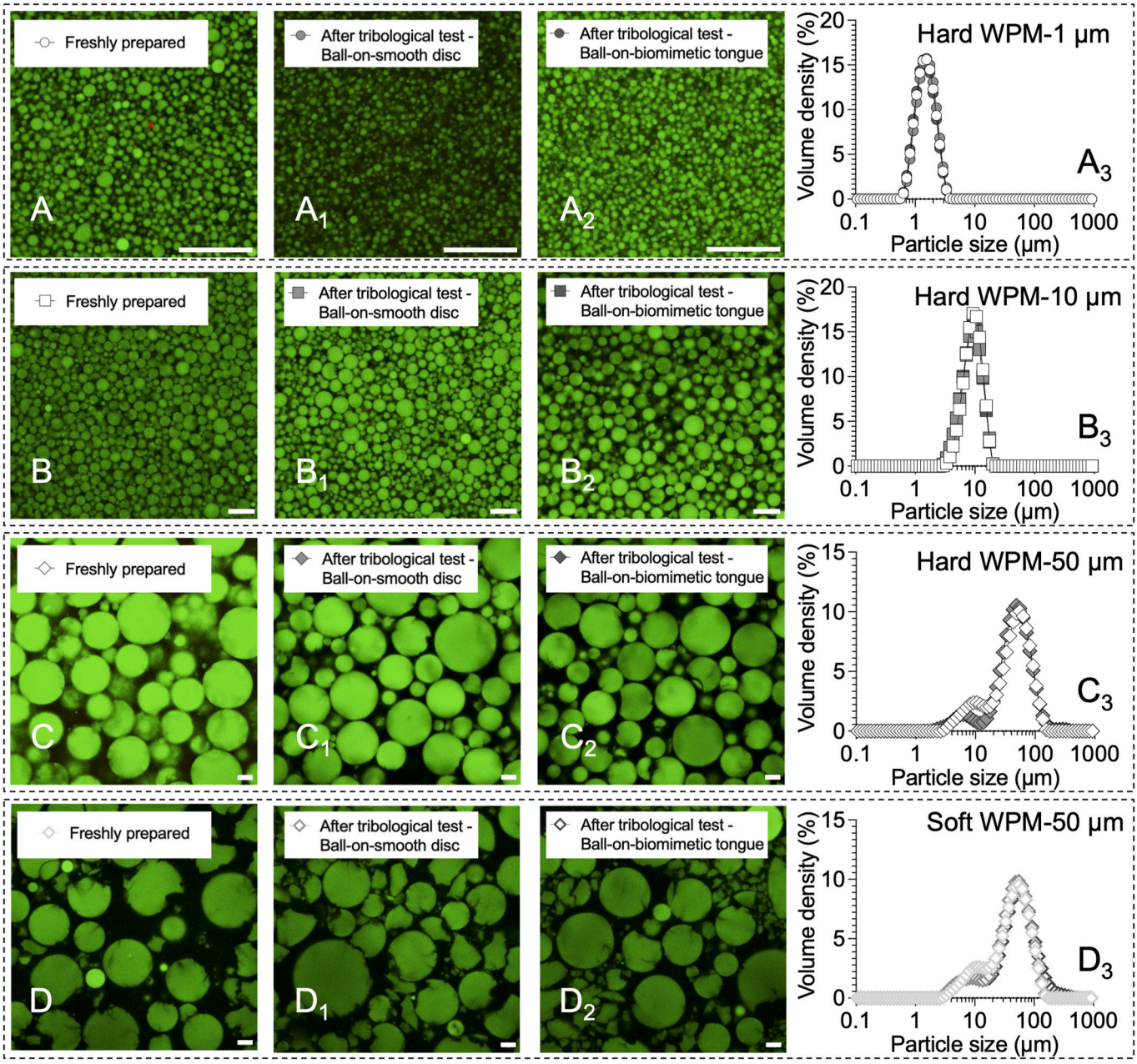

Fig. 2. Confocal images of WPM dispersions at a particle volume fraction of 12 vol %. Confocal image of freshly prepared *hard* WPM - 1 μm (A), *hard* WPM - 10 μm (B), *hard* WPM - 50 μm (C) and *soft* WPM - 50 μm; (1) and (2) are the confocal images of the WPM samples in the row, after tribological shear under ball-on-smooth disc and ball-on-biomimetic tongue setups, respectively. Mean particle size distribution of WPM before and after tribological shear using both smooth and biomimetic tongue surface. The white scale bars in the images represent 20 μm. The green color represents protein stained by Fast Green in the confocal micrographs (A-D_2). (For interpretation of the references to color in this figure legend, the reader is referred to the Web version of this article.)

previously reported value (Andablo-Reyes et al., 2019), and increased to about 85 kPa after 60 min of heating. This time-dependent rise in G′ reflects the well-documented behavior of heat-set WPI gels, which continue to stiffen with heating and reaches plateau after roughly 20 h (Verheul & Roefs, 1998). Nevertheless, given the nearly fourfold difference in G' in the parent gel with difference in protein levels, we therefore, refer to the WPM fabricated with 15 wt % and 25 wt % protein as *soft* and *hard* WPM, respectively.

3.3. Flow behavior of WPM dispersions

The shear flow behavior of dispersions influences the drag forces required to entrain the particles which generate hydrodynamic forces required to separate tribological contacts, a phenomenon that plays a critical role in modulating the lubrication performance of particulate system. Due to the density mismatch between WPM and dispersion medium, it has been suggested that the flow sweeps should be conducted at sufficiently high shear stresses to ensure particle's resuspension. This stress threshold for avoiding sedimentation can be estimated using the dimensionless Shields parameter (*Sh*), defined as the ratio of the fluid force acting on the particle to the particle's weight (Lobry et al., 2019; Papadopoulou et al., 2020), Therefore, only the data points obtained at shear stresses exceeding the threshold ($Sh = 1$) are indicated by filled symbols in Fig. 3.

The change in the apparent viscosity of WPM dispersions as a function of volume fraction (φ) is shown in Fig. 3. The viscosity of WPM

Table 1
Mean particle size ($D_{4,3}$) of WPM collected before and after tribological measurements. The data are shown as means and standard deviation of triplicate samples (n = 3 × 1).

Sample	Freshly prepared	After tribological measurements		*p value*
		Smooth surface	Biomimetic tongue	
hard WPM – 1 μm	1.57 ± 0.04	1.614 ± 0.04	1.45 ± 0.01	<0.01
hard WPM – 10 μm	9.59 ± 0.18	9.30 ± 0.24	9.25 ± 0.16	<0.05
hard WPM – 50 μm	47.28 ± 0.23	50.56 ± 1.00	51.02 ± 0.44	<0.01
soft WPM – 50 μm	47.14 ± 1.02	49.48 ± 1.46	58.32 ± 0.81	<0.01

dispersions exhibits a similar dependency on φ, such that increasing φ consistently leads to higher viscosity across the presented shear rate range (1–500 s^{-1}). Notably, the transition from $\varphi = 24$ to 48 vol% results in a significant increase in viscosity for WPM-10 μm and (*soft*/*hard*) WPM-50 μm dispersions. This observation may be explained by the microgels reaching their random packing limit; consequently, the WPM dispersion behaves predominantly as a viscous fluid. Although it is well established that the limit of close-packing fraction for micron-sized particles is around 64 %, this value can be varied with shape, elasticity, and dispersing matrix (Brown et al., 2011; Genovese, 2012; Kew et al., 2023; Sarkar et al., 2017). For instance, glass spheres in glycerol reach a packing limit about 60 vol %, but dropped to near 33 vol % in mineral oil due to aggregate formation (Papadopoulou et al., 2020). Another possible explanation might involve microgel jamming effect, which describes a mechanical transitions of packed structure transits from a liquid to a solid-like state, leading to higher interparticle resistance to movement and contributing to increased viscosity (Chu et al., 2024; Kew et al., 2023; Nikolov et al., 2020). Microgels, being soft, fuzzy, and interpenetrable, might blur the line between the two (Nikolov et al., 2020). The increase in viscosity in the current case might suggest some sort of interpenetration of WPM as they are forced and sheared together at higher φ, effectively increasing viscosity with enhanced interparticle interaction.

Interestingly, *soft* WPM dispersions display higher viscosity than their hard counterparts at φ of 24 % and 48 %, contrary to the earlier finding indicating that higher microgel elasticity tends to increase dispersions viscosity (Andablo-Reyes et al., 2019). It perhaps should be noted that the φ in the present study were calculated based on the assumption that the density of WPM equals that of the corresponding WPI solution. This method does not account for any potential solvent release from the cross-linked protein hydrogel or microgel shrinkage, subsequent redispersion in buffer may cause microgel to rehydrate, hence a density change. It is difficult to accurately measure the effective φ of the particles. Hence, we hypothesize that *soft* WPM-50 μm dispersions might have a higher effective φ than *hard* WPM-50 μm as the deformable ones allows denser packing and partial interpenetration as compared to the harder counterpart.

On the other hand, WPM dispersions at lower φ (3, 6, and 12 vol %) exhibit near-Newtonian behavior, as indicated by their shear rate-independent viscosity, suggesting that WPM are likely behave as discrete individual spheres with minimal interparticle interactions, due

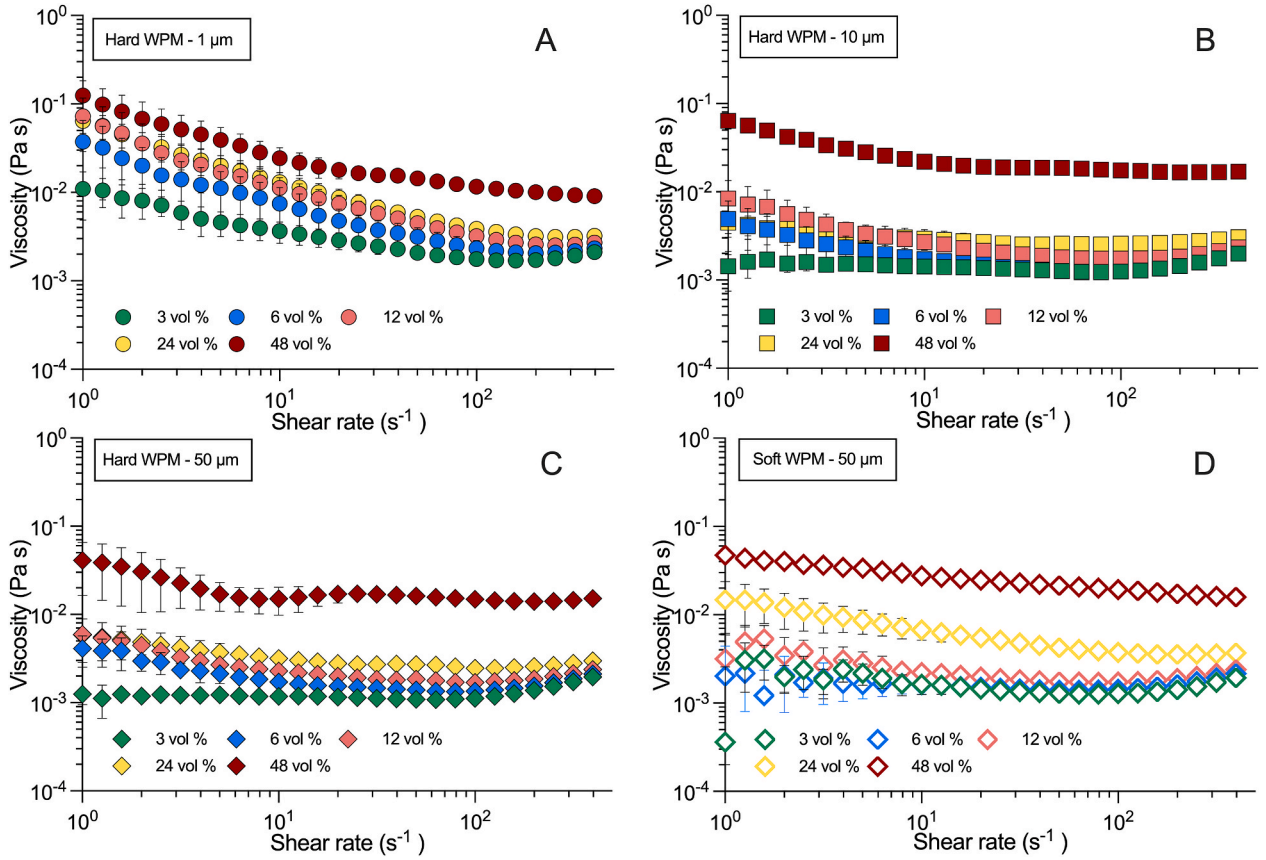

Fig. 3. Apparent viscosities of various volume fractions of WPM dispersions as a function of shear rate showing the effect of particle size (A–C) and modulus (C–D) of WPM. Microgels made from 25 wt % whey protein solution with an average diameter $D_{4,3}$ of 1, 10 and 50 μm were abbreviated as *hard* WPM - 1 μm (A), *hard* WPM - 10 μm (B), and *hard* WPM - 50 μm (C) for microgels of different sizes, respectively. *Soft* WPM - 50 μm refers to microgel particles made from 15 wt % whey protein solution with a size of 50 μm (D). The pellets collected after centrifugation are considered as 100 vol%; lower volume fractions of microgels (3–48 vol %) were obtained by redispersing the pellets in 20 mM PBS buffer. Data are plotted as means and standard deviation shown as error bars of triplicate samples (n = 3 × 1).

to the weak van der Waals forces (Gabriele et al., 2010). However, an exception is observed in *hard* WPM-1 μm dispersions, which exhibit typical shear thinning behavior, even at the lowest φ (3 vol %). This observation suggests that there might be presence of loosely aggregated WPM clusters held together by weak bonds at lower shear rates, which undergo structural disintegration under extreme shear conditions. Another possible contributing factor to this behavior is the influence of Brownian motion. The relative importance of diffusion compared to hydrodynamic effects can be evaluated using the Péclet number *(Pe)* (Brenner, 1974; Stickel & Powell, 2005), which is defined as:

$$Pe = 6\pi\gamma\eta_s {d_H}^3 / 8k_B T, \quad (4)$$

where, η_s represents the dispersing medium viscosity, d_H denotes the hydrodynamic diameter of the WPM, k_B is the Boltzmann constant (1.3807×10^{-23} J/K), and $T = 297$ K. Based on the shear rates ($\dot{\gamma}$) studied (1-500 s^{-1}) and the dispersing medium viscosity of 0.0008 Pa s, the *Pe* number for WPM dispersion with particle size of 1 μm ranges from 0.4 to 92, whereas it ranges from 4×10^3 to 9×10^4 for *hard* WPM-10 μm and from 5×10^4 to 1×10^8 for *hard* WPM-50 μm particles dispersed in buffer, respectively. These *Pe* values are sufficiently large to assume that the effect of Brownian motion is negligible for the *hard* WPM-10/50 μm dispersions. On the other hand, for *hard* WPM-1 μm dispersions, their rheological responses may be significantly influenced by Brownian motion. This can suggest similar characteristic times for flow and Brownian diffusion processes for *hard* WPM-10/50 μm and hence the greater tendency of *hard* WPM-1 to shear thin as the shear rate increases, as observed in Fig. 3 (Soltanahmadi et al., 2022). The slight increase in viscosity observed in all WPM dispersions with lower volume fractions at higher shear rates is likely an artifact of the instrument, as these low stresses approach the rheometer's limits for accurate measurements. Thus, at the end of the shear thinning region, the infinite shear viscosity value (η_∞), at the second Newtonian plateau, measured at a shear rate of 158 s^{-1}, was then adopted for scaling the lubrication performance of WPM dispersions.

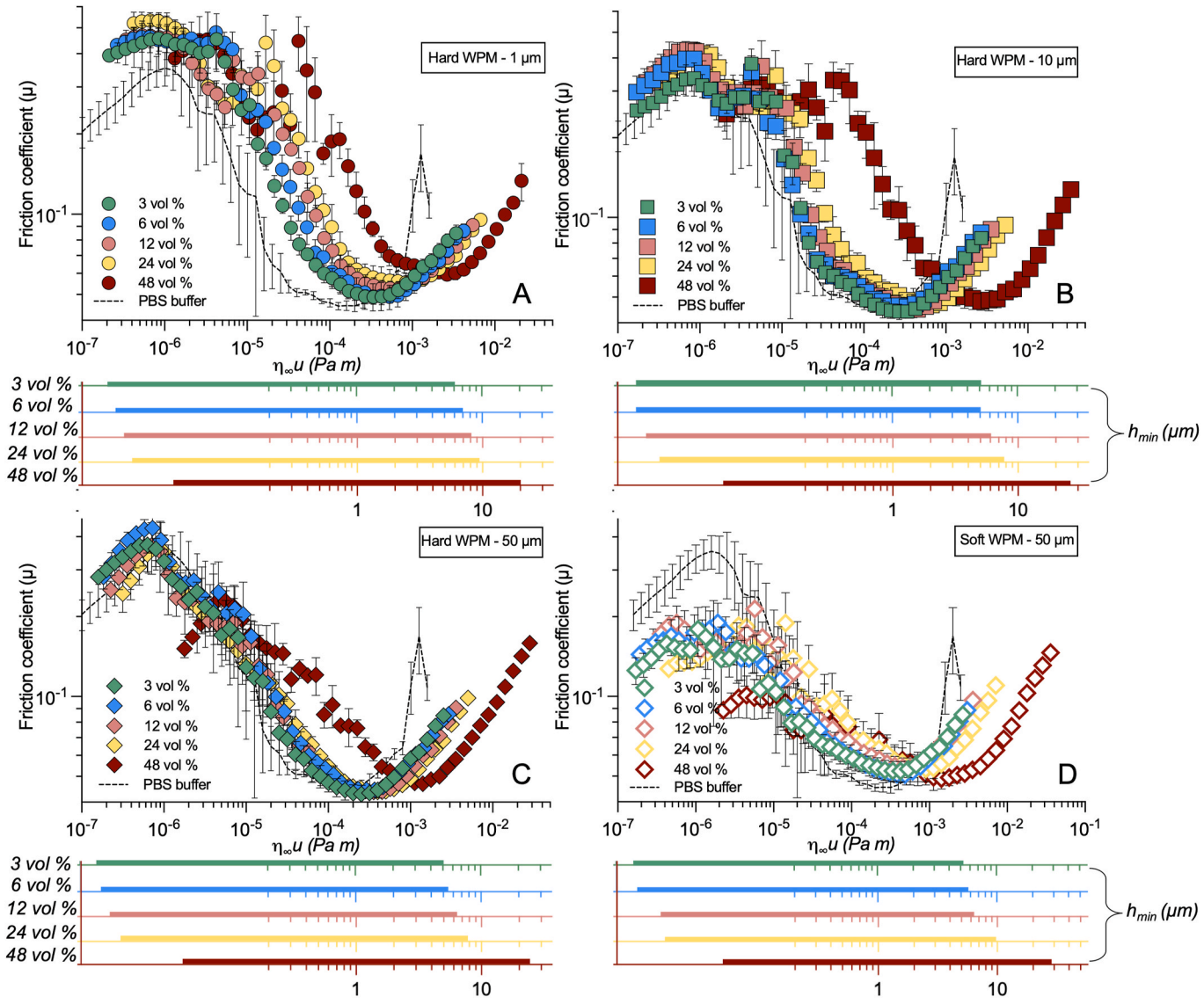

Fig. 4. Stribeck curves of WPM dispersions under a ball-on-smooth disc configuration of various volume fractions (3–48 vol %) of *hard* WPM dispersions with different particle volume fractions and sizes 1 μm (A), 10 μm (B), 50 μm (C), respectively, and 50 μm *soft* WPM dispersions (D). Friction coefficients are plotted against a combined factor of the entrainment speed and the infinite plateau viscosity (η_∞). The minimum film thickness (h_{min}) predicted across the tested speeds range are shown beneath the friction curve image. Phosphate buffer saline (PBS) is shown as control. Data are plotted as means and standard deviation shown as error bars of triplicate samples (n = 3 × 1).

3.4. Soft tribology of WPM dispersions in a ball-on-smooth disc setup

The friction curves obtained using a ball-on-smooth disc configuration for WPM dispersions with varied φ (3–48 vol %) are shown in Fig. 4, where friction coefficient is plotted as a combined factor of velocity and viscosity. The Stribeck curve of PBS buffer was also included for reference. In agreement with previous findings, the friction behavior of simple Newtonian fluid without surface active agents at the interface exhibits typical Stribeck lubrication pattern, where the boundary, mixed, and hydrodynamic lubrication regime are clearly identified (Bongaerts et al., 2007; Rudge et al., 2023). Fig. 4A shows the friction coefficients of *hard* WPM-1μm dispersions. The introduction of *hard* WPM-1μm to the buffer slightly increased friction coefficients in the boundary and mixed regimes, even at the lowest φ, suggesting that the presence of particles influences the friction response, particularly when surfaces are in close proximity. At higher $U\eta_\infty$ numbers, the friction curves for the dispersions of *hard* WPM-1 μm and buffer partially overlapped in the elasto-hydrodynamic lubrication (EHL) regime. This observation suggests that the lubrication performance of *hard* WPM-1 μm in the EHL regime can be approximated as Newtonian fluids, which is predominantly governed by the viscous drag.

Theoretically, boundary lubrication occurs when lubricant films are fully expelled from the contact interface, resulting in direct surface-surface interactions that maximize the traction resistance (Chen & Stokes, 2012; Sarkar, et al., 2019, 2021; Stokes et al., 2013). Thus, the lubrication mechanism of fluids devoid of surface-active components are governed by the surface characteristics of tribopair across both molecular and microscale dimensions. Boundary lubrication *via* particle entrapment arises from particle-tribopair adsorption (Sarkar et al., 2017; Yakubov et al., 2015), tribopair deformation (Hirano & Yamamoto, 1959; Yakubov et al., 2015), and particle aggregation (Wu, et al., 2015, 2017), all of which collectively increase the effective film thickness and reduce direct contacts between the tribopairs. However, the particle entrapment is influenced by the ratio between particle dimensions and the lubrication gap size, a parameter dynamically modulated by hydrodynamic lift forces and tribopair deformation (De Vicente et al., 2005; Myant et al., 2010; Spikes, 2015). To demonstrate the particle versus film thickness relationship, the lubricant film thickness across the Stribeck lubrication regime was systematically analyzed using Equation (5):

$$\frac{h_m}{R'} = \overline{H}_m = 2.8\overline{U}^{0.65}\overline{W}^{-0.21} \quad (5)$$

In equation (5), the dimensionless speed and load are defined by equations (6) and (7), where U is the entrainment velocity, W is the applied load, η is the viscosity of the WPM dispersion, R' is the reduced radius in the entrainment direction, defined by $1/R' = 1/R_X + 1/R_y$, and E' is the reduced elastic modulus, defined by $2/E' = (1-\nu_1^2)/E_1 + (1-\nu_2^2)/E_2$.

$$\overline{U} = \frac{U\eta}{E'R'} \quad (6)$$

$$\overline{W} = \frac{W}{E'R'^2} \quad (7)$$

The minimum film thickness (h_m) for the WPM dispersion-lubricated contact was calculated using the modified Hamrock-Dowson empirical formulation (De Vicente et al., 2005; Hamrock & Dowson, 1977). The selection of h_m rather than central film thickness is justified by its better representation of actual lubricant film thickness in the boundary and mixed regime, where asperity contact dominates (Soltanahmadi et al., 2022). The estimated h_m values are presented below the *X-axes* in Fig. 4. For the *hard* WPM-1 μm dispersion with varying φ from 3 to 24 vol %, the h_m value at the transition point from mixed to hydrodynamic regime were 1.17–1.73 μm. Therefore, beyond this critical transition point, WPM may be expected to freely entrain in between the tribopairs, accounting for the observed overlapping between the dispersion's friction curves and the buffer solution in Fig. 4A. The film thickness calculated in the boundary and mixed regime is expected to be relatively lower than the particle size. Strikingly, the friction coefficients of *hard* WPM-1 μm dispersions were higher than those of the buffer and exhibit a dependency on φ, with the highest φ yielding the greatest friction, as depicted in Fig. 4A. This suggests that particle entrapment is significant in this system. This observation aligns with previous study demonstrating that rigid particle can become entrapped between soft tribopair and potentially deform contact surfaces locally even at the lowest entrainment velocity, a phenomenon likely attributed to differences in elastic modulus between the two interacting bodies (Yakubov et al., 2015). Similarly, given that the elastic modulus of the particles is three times that of the elastomer, particle entrapment might also be attributed to the tribopair deformation induced entrapment.

The counterintuitive part here is the delubrication effect with particle entrapment. In fact, the tribological responses (*i.e.,* lubrication enhancement *vs.* delubrication) of the rigid particle entrapment remains largely ambiguous in literature and appears to be system dependent. In soft hydrophobic PDMS-PDMS contacts, where intrinsic adhesive friction dominate (Chernyak & Leonov, 1986), inclusion of rigid particles modifies interfacial topography through localized substrate deformation. This effectively creates surface asperities that reduces direct contact in contact region, thereby reducing friction (Yakubov et al., 2015). However, in soft hydrophilic contacts or facing cases where dispersing medium itself provides superior lubrication (*e.g.*, saliva), the particle inclusion can disrupt the formation of a hydration layer, inducing a delubrication effect by premature aqueous film rupture (Chojnicka-Paszun et al., 2014; De Wijk et al., 2006). Moreover, roughness amplification driven by particle inclusion might be associated with lubricant replenishment failure and accelerated fluid drainage in the contact region, synergistically increasing friction (Selway et al., 2017).

It is worth noting that the tribopair used in the current study comprises of three glass hemispheres and wettability-modified silicone elastomer. The friction coefficients of PBS buffer in the boundary regime measures about 0.3, which is significantly lower than typical PDMS-PDMS contacts ($\mu > 1$) and also lower than the Milli-Q water (see Supporting Fig. S3A). In fact, the sodium ions are expected to enhance aqueous lubrication by forming an anchored hydrated layer that maintains interfacial separation and bearing load (Garrec & Norton, 2012; Raviv & Klein, 2002). This process may involve the Hofmeister effect, as evidenced by the considerable decrease in boundary friction coefficients observed with increasing salt concentration in a conventional ball-on-disc tribometer (Garrec et al., 2012). This lubrication enhancement can be mechanistically explained by the repulsive effect of hydrated anions, which increases the minimum surface separation distance by overcoming interfacial van der Waals attractions, this separation in turn, provide spaces for water molecules accommodation and retention, enhances localized viscosity (Garrec et al., 2012; Raviv et al., 2002). Therefore, we hypothesize that there is an aqueous lubricating layer may be attributed to both hydrophilic glass surface-water molecule interaction and the formation of ionic hydration layers follow Hofmeister series effect. The inclusion of *hard* WPM is likely to indent the substrate and create additional asperities, causing higher surface resistance and the disruption of effective boundary lubrication film buildup. This effect continued with increasing φ, as the higher entrapment density progressively disrupted or even replaced boundary film with asperities contact, and ultimately leads to a delubricating effect.

Turning to larger particles (*i.e.*, *hard* WPM-10/50 μm), the friction coefficients at low φ ($\leq$24 vol %) only show minor deviation with the buffer, especially for hard WPM-50 μm dispersions (Fig. 4B and C). It should be noted that the minimum film thickness for *hard* WPM-10 μm and *hard* WPM-50 μm dispersions ($\varphi = 0.24$) estimated at the transition from the mixed to hydrodynamic regime were 1.82 and 1.51 μm, respectively. These values were more than one order of magnitude smaller than the *hard* WPM-10 μm and nearly two orders below the *hard*

WPM-50 μm particle dimension. This suggests that large particles would not be able to entrain into the contact interface.

In Fig. 4B, the friction curves of *hard* WPM-10 μm dispersions exhibited two peaks at low $U\eta_\infty$ values. A similar dual-peak pattern appeared for hard WPM-1 μm, becoming more pronounced at higher volume fractions (48 vol %, Fig. 5A and a). The first likely corresponds to the running in phase, modulated by the deformation or removal of projecting irregularities from the contact (Blau, 2005; Myshkin et al., 2005). The reason for the subsequent reduction in friction is unclear but may be due to WPM accumulation outside the contact region. This buildup could hinder effective lubricant entrainment and lead to a slight increase in friction, particularly in tribopairs operating under a pure sliding mechanism (Rudge, et al., 2020, 2025). The entrainment dynamics described above was not observed for *hard* WPM-50 μm dispersions (Fig. 4C). Instead, the friction curves exhibited only a trivial shift relative to the buffer, suggesting that larger particles are less efficient at migrating into and replenishing the confined wedge at the contact inlet. Consequently, the effect of particle accumulation and subsequent blockage of fluid flow is marginal.

It is noteworthy that, irrespective of *hard* WPM's dimension, the highest φ (48 %) leads to a significant increase in the dispersion's viscosity (see the sudden jump of viscosity from 24 to 48 vol % in Supporting Fig. S4). Thus, a significant shifting of friction curves to higher $U\eta_\infty$ value was observed for the dispersions at 48 vol %. Although differences in the protein microgel fabrication methodologies, similar results were reported by Kew et al. (2023); Sarkar et al. (2017) and Chu et al. (2024), which possibly resulted from particle aggregation or jamming. Thus, the increased friction can be attributed to the densely packed microgel impeding effective fluid replenishment, surface motion as well as hydrodynamic lifting buildup at the interfaces.

Fig. 4D shows the Stribeck curves for *soft* WPM 50 μm dispersions at varying volume fractions, with clear transitions from boundary through mixed to hydrodynamic lubrication regimes. To assess the effect of particle deformability, we directly compared these curves with those obtained for *hard* WPM of the same size (Fig. 5B and b). Interestingly, despite the particle size being several orders of magnitude larger than the h_m, *soft* WPM gave much lower friction coefficients in boundary regime compared to buffer alone, suggesting the *soft* WPM could effectively deform under high tribological shear and entrain into the contact interface (Sarkar et al., 2017; Soltanahmadi et al., 2022). Of more importance, the highest φ yields the most pronounced enhancement in boundary lubrication, likely because of the higher proportion of WPM at the contact interface ensuring microgel replenishment. Generally, increased particle hardness is reported to reduce friction, as evidenced by the studies on fluid gel, gelatin particle and WPM dispersions (Andablo-Reyes et al., 2019; Gabriele et al., 2010; Garrec et al., 2013; Rudge et al., 2020). In these cases, the modulus of particles have been typically several orders of magnitude lower than that of the contact materials (*e.g.*, PDMS or glass). Therefore, rather than tribopair indentation, particle deformation and surface separation *via* an aqueous lubricant film made up of flattened microgels appear to be responsible for the observed friction coefficients reduction (Torres et al., 2018).

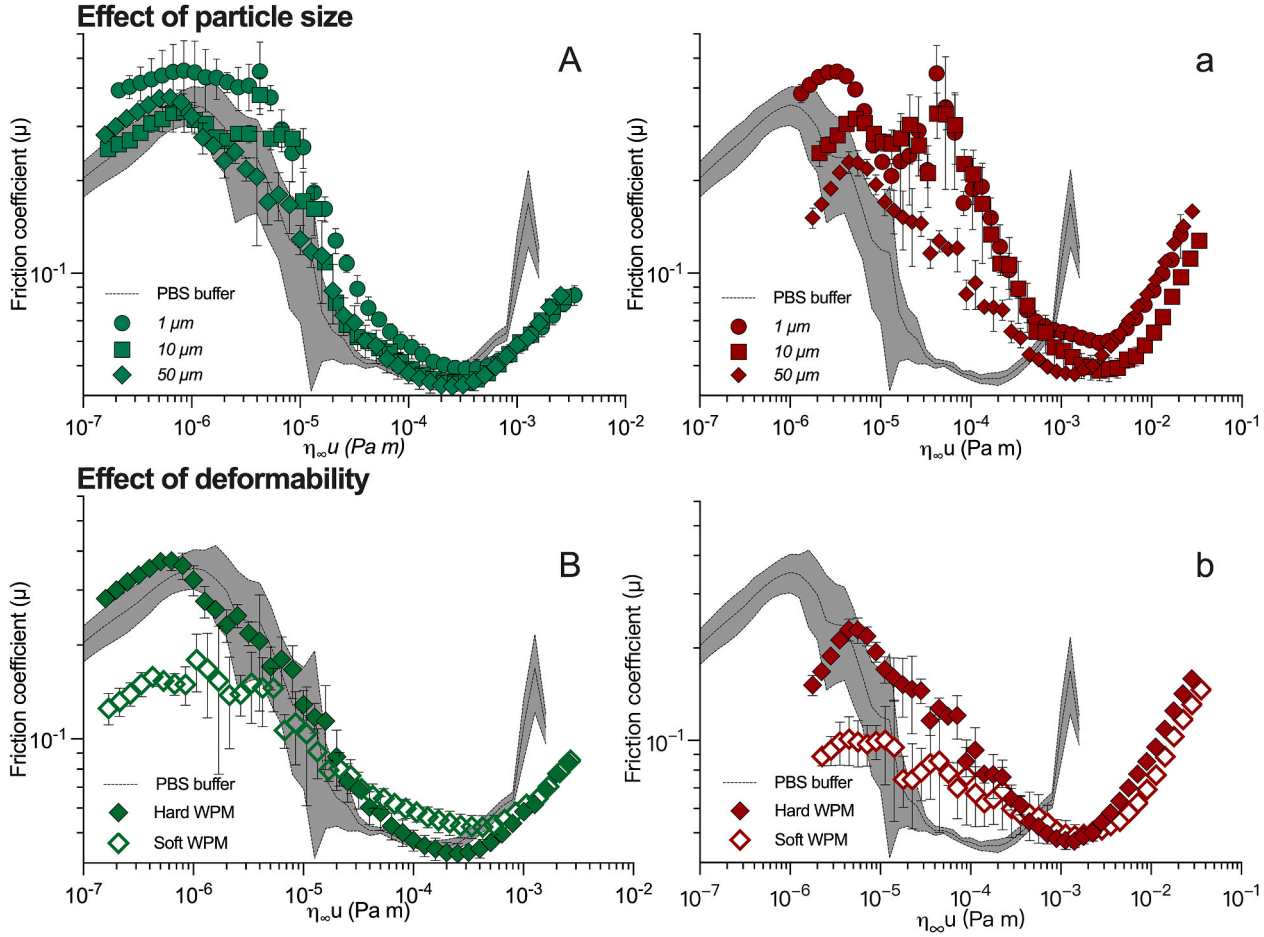

Fig. 5. Stribeck curves of WPM dispersions under ball-on-smooth disc configurations. Friction curves of WPM with varied particle sizes (1, 10, and 50 μm) at volume fractions of 3 vol % (A) and 48 vol % (a). Friction curves of WPM with varied elastic modulus (85 kPa versus 350 kPa) at volume fractions of 3 vol % (B) and 48 vol % (b). Friction coefficients are plotted against a combined factor of the entrainment speed and the infinite plateau viscosity (η_∞). Phosphate buffer saline (PBS) is shown as control. Data are plotted as means and standard deviation shown as error bars of triplicate samples (n = 3 × 1).

Changes in microgel modulus did not affect the overall lubrication performance in the mixed and hydrodynamic regimes across the φ range (see Fig. 5B and b). However, the data in Fig. 5b indicates a delubrication effect at the highest φ (48 %) compared to buffer, mirroring the behavior of the *hard* WPM 50 μm dispersions. This observation may also result from jamming effect that restricts effective dispersing phase entrainment. An alternative explanation is that high surface shear may induce intraparticle interpenetration and diffusion, potentially promoting shear-induced aggregation of microgels. This is supported by the observed significant increase in particle size after tribological measurements, particularly for *soft* WPM (Table 1), which likely reflects enhanced particle-particle or particle-substrate adhesion and, consequently, higher friction coefficients.

Together, we reveal a novel outcome in which WPM attempt to lubricate a soft elastomer surface with a high affinity for the aqueous phase schematically shown in Fig. 6. The entrapment of *hard* WPM (in comparison to the tribopair) occurs only when the separation distance (h_m in EHL regime) approaches the particle dimensions. This particle confinement is likely accompanied by elastic indentation of the substrate, which disrupts aqueous lubrication by creating asperities. Thus, under these conditions, *hard* WPM act as *delubricants*. In contrast, relatively *soft* WPM of the same dimensions dramatically reduce boundary friction coefficients, a phenomenon attributable to their deformability. The experiments also shows that lubrication can be further compromised by jamming effect with particle close packing at higher φ, restricting effective fluid entrainment. To our knowledge, this is first report on micron-sized WPM showing effect of size and deformability in smooth, soft and hydrophilic contacts.

3.5. Soft tribology of WPM dispersions in ball-on-biomimetic tongue setup

To gain insight into the capability of WPM dispersions to lubricate surfaces that emulate the topography, deformability, and wettability of real human tongues, tribology measurements were conducted in a ball-on-biomimetic tongue setup. A notable observation is the substantially lower friction coefficients at low $U\eta_\infty$ (1.00×10^{-7} – 6.36×10^{-6}), followed by higher friction in the elevated $U\eta_\infty$ range (6.36×10^{-6} – 1.60×10^{-3}), compared to smooth surfaces. These trends correspond to the boundary and mixed lubrication regimes, respectively, observed on the smooth substrate (Supporting Fig. S3C). As mentioned before, the boundary lubrication is believed to be more about a surface-dominated regime, with minimal amount of lubricant present in contact region for typical smooth contacts. Similar principles are also applicable to the micro-papillated surface in this biomimetic tongue-like setup, where measured friction force at lower speeds primarily reflects the cumulative shear stresses at each individual papillae-ball contacts (Andablo-Reyes et al., 2020; Soltanahmadi et al., 2022). Assuming Tresca friction, where the friction force is proportional to the real contact area, the observed reduction in friction under Newtonian fluid (buffer) lubrication is likely due to a decreased real contact area, as the glass hemispheres can be rested on a limited number of papillae-mimicking domes and cylinders, thus minimizing adhesive dissipation (Peng et al., 2021; Ranc et al., 2006; Taylor & Mills, 2020; Xu et al., 2021). An alternative reason, mediated by fluid entrapped within inter-papillated lubricant reservoir, might generate hydrostatic reaction lift forces that maintain a thick lubricating film between tribopairs under a near-static condition, bearing the load and enhancing lubrication (Bhushan, 2013; Peng et al., 2021; Soltanahmadi et al., 2022; Zou et al., 2022).

Fig. 7 presents the Stribeck curves for all WPM dispersions alongside the PBS buffer. Noteworthy, a pronounced delubricating effect with WPM involvement was observed, as φ increased with friction coefficient increasing, regardless of particle size and elastic modulus. The detrimental role of *hard* WPM inclusion on aqueous lubrication was discussed in our previous section on a ball-on-smooth surface setup, where entrainment is restricted to cases in which the particle size matches h_m. The h_m for a traditional ball-on-disc setup is established from asperities level to several microns. In contrast to smooth substrates, current observation implies that WPM are entrained indiscriminately on the biomimetic tongue, which largely attributed to its distinct interfacial architecture. As schematically illustrated in Fig. 8A, the papillae indentation would create two separate spaces potentially available for microgel accommodation. The thickness of the upper layer of deformation is defined by the height difference between intact and fully deformed papillae, while the lower layer acts as a reservoir and its thickness is defined by the height of the deformed papillae. During sliding, the upper layer experiences a dynamic condition in which the ball continuously collides with and deforms the papillae while releasing previously confined ones. WPM dispersed in the upper layer are expected to participate in this papillae deformation process and contribute to lubrication, so long as the indentation of papillae exceeds the particle size of WPM. While the lower layer remains relatively static, lubrication is only expected to be affected when its thickness decreases to a value comparable to or less than the particle size, allowing particles to interact with the bottom surface by sedimentation or *via* high shear induced entrainment. Therefore, we postulate that the reason behind WPM entrainment under the conditions that realistically mimic tongue-palate

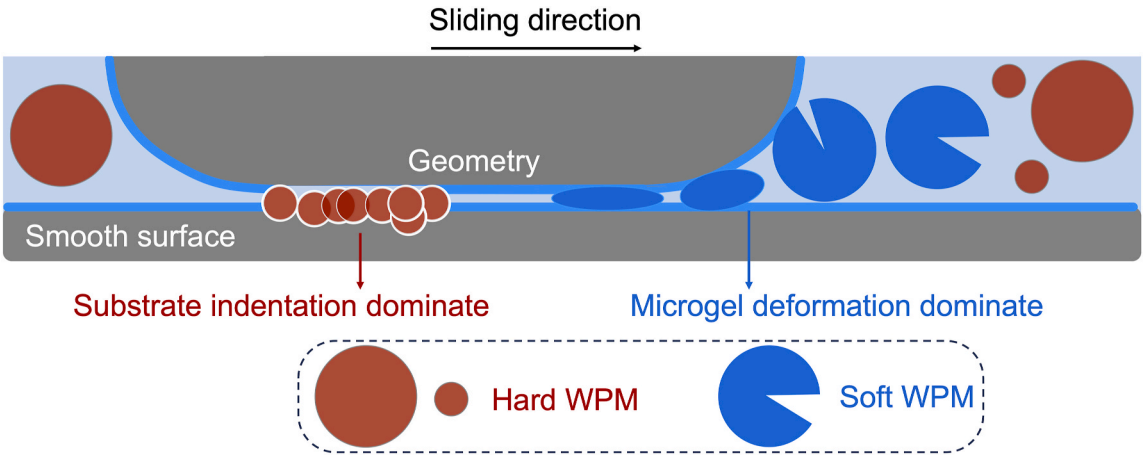

Fig. 6. Schematic illustration of entrapment mechanisms of microgel in a ball-on-smooth disc setup. The blue layer attached to the tribopair surface indicates the aqueous lubrication film. Microgels are classified as "*hard*" or "*soft*" based on a comparison of their elastic modulus with respect to the tribopair material. *Hard* WPM become entrapped *via* substrate indentation, which impedes effective aqueous lubrication. The enhanced deformability of *soft* WPM facilitates their entrapment and promote lubrication by bearing the load without disrupted the lubricating film. (For interpretation of the references to color in this figure legend, the reader is referred to the Web version of this article.)

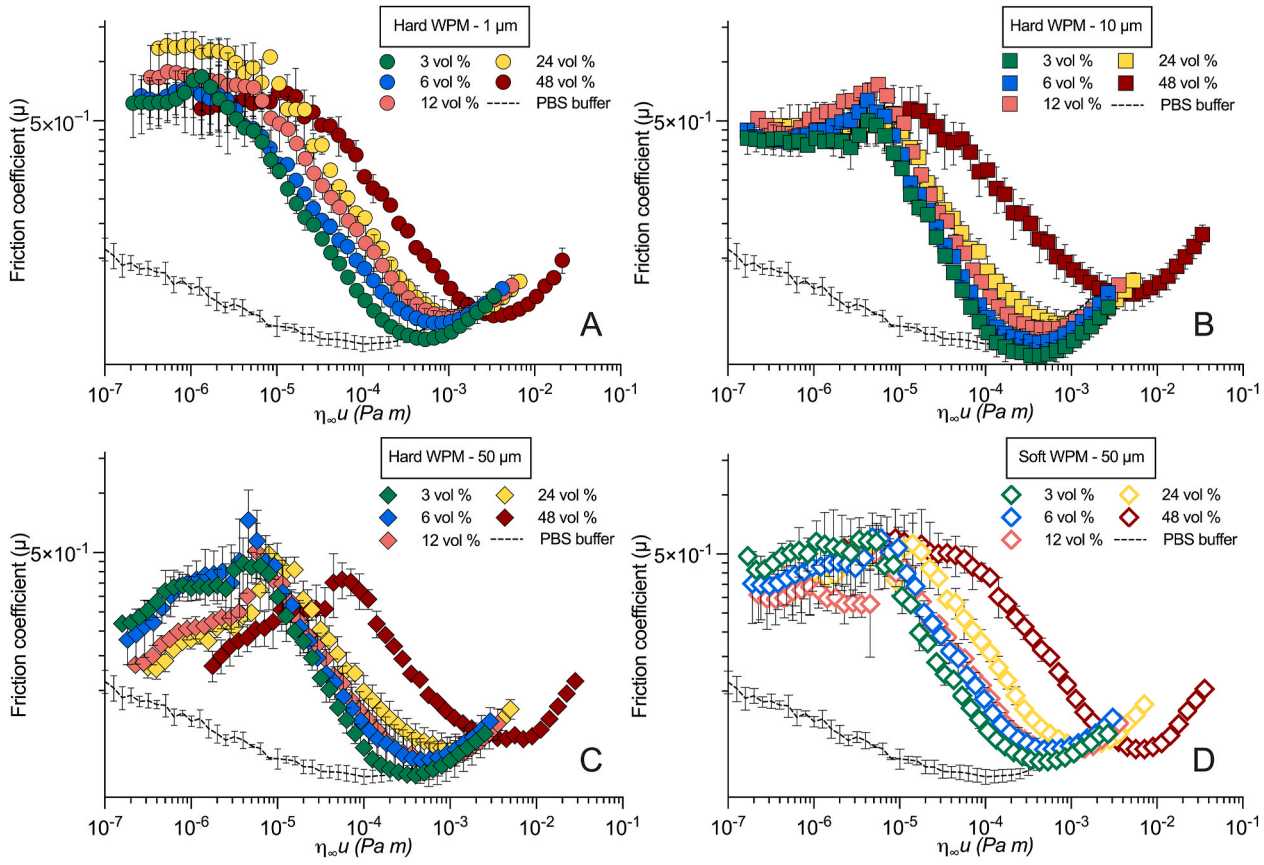

Fig. 7. Stribeck curves of WPM dispersions under a ball-on-biomimetic tongue configuration with friction curves of various volume fractions (3–48 vol%) of *hard* WPM dispersions with different particle volume fractions and sizes 1 μm (A), 10 μm (B), 50 μm (C), respectively, and 50 μm *soft* WPM dispersions (D). Friction coefficients are plotted against a combined factor of the entrainment speed and the infinite plateau viscosity (η_∞). Phosphate buffer saline (PBS) is shown as control. Data are plotted as means and standard deviation shown as error bars of triplicate samples (n = 3 × 1).

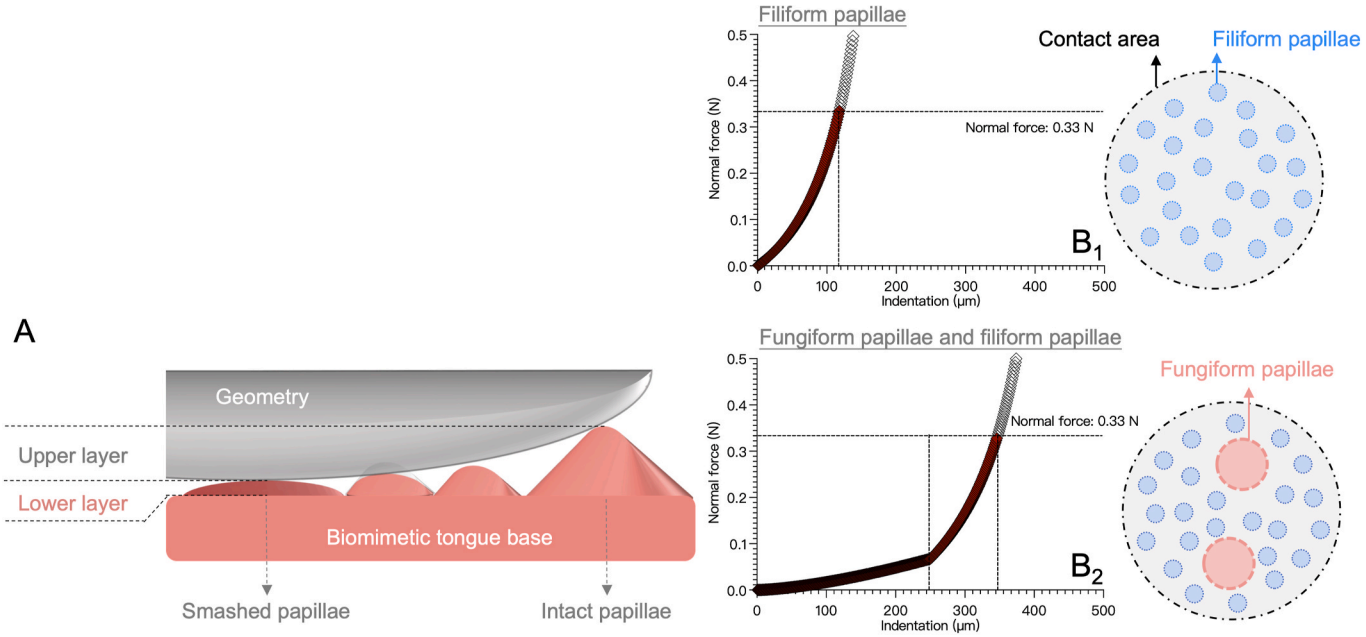

Fig. 8. Schematic illustration defining the upper and lower layers of deformation created by papillae indentation (A). The upper layer is characterized by the height difference between intact and deformed papillae, while the lower layer corresponds to the region occupied by the deformed papillae. Two potential scenarios describe how the applied load (0.33 N) is distributed and how the papillae are indented: the applied load is distributed solely among the filiform papillae (B_1) or between fungiform and filiform papillae (B_2). The accompanying top-view inset shows the relative dimensions of the estimated contact area and papilla diameter.

interactions is related to the interplay between the thickness of these two layers largely dominated by papillae deformation as well as the microgel dimensions.

The extent of papillae deformation not only determines the thickness of two layers, which in turn, also decide whether WPM can be involved into the ball-papillae frictional dissipation. Drawing a theoretical approximation of the ball-papillae contact mechanisms is therefore crucial to understand their interactions. It should be noted that the papillated structure on biomimetic tongue may exhibit viscoelastic hysteresis, resulting in incomplete recovery between consecutive sliding cycles, a phenomenon that is likely at higher sliding velocities. Such dynamic deformation and relaxation of the asperities could modify the film thickness of upper layer over time. Although this effect was not addressed in the present study, we recommend that future work explicitly quantify these hysteretic losses and their impact on film stability. Considering that the dimension of glass hemisphere is orders of magnitude larger than both types of papillae, the contact was simplified by approximating the scenario as a flat plane compressing the dome (representing the fungiform) and pillar (representing the filiform) structures. We mirrored the biomimetic tongue-on-flat surface setup, where papillae deformation was estimated using Hertz contact theory and Hencky strain by modeling fungiform papillae as hemispheres and filiform papillae as cylinders (Andablo-Reyes et al., 2020).

The effective contact area of the flat plane was estimated using Hertzian analysis for a ball-on-smooth disc setup under a normal load of 0.33 N, and the extent of papillae participation was determined based on their density (9 fungiform and 160 filiform per cm^2). In a classic point contact, the compliant contact area can be defined by equations (8) and (9). The E_1, E_2 and ν_1, ν_2 represent the Young's modulus and Poisson's ratio respectively, where the E_1 and ν_1 of glass are assumed to be 70 GPa and 0.17, and the E_1 and ν_1 of Eco-flex elastomer are 120 kPa and 0.5. The radius of contact between a hemisphere with a half-space plane given a contact radius of 2.16 mm and an apparent contact area of 14.65 mm^2 under a surface load of 0.33 N. Consequently, the estimated papillae inclusion comprised 24 filiform and 2 fungiform papillae.

$$aHertz = \left(\frac{3\,PR}{4E'}\right)^{\frac{1}{3}}; \tag{8}$$

$$\frac{1}{E'} = \frac{1}{2}\left(\frac{1-\nu_1{}^2}{E_1} + \frac{1-\nu_2{}^2}{E_2}\right). \tag{9}$$

The apparent contact area for each filiform papillae was estimated as the base area of a cylinder with a diameter of 350 μm (Andablo-Reyes et al., 2020). Meanwhile, the contact area of each fungiform papillae was determined using Hertzian contact theory for a hemisphere in contact with a half-space, yielding an area of 0.54 mm^2 per papillae. Collectively, these contributions yield a contact area of 2.85 mm^2, which is significantly lower than that observed in a ball-on-smooth disc setup, explaining the observed reduction in boundary friction for the buffer solution.

Similarly, taking a simplified model of a flat plane loading upon the papillae, the indentation is estimated as follows: the applied load (0.33 N) is likely distributed either between both types of papillae (fungiform and filiform, see Fig. 8B_2) or solely among the filiform papillae, given their significantly higher density (Fig. 8B_1). Considering that the height of the fungiform papillae is twice that of the filiform papillae and that their density is approximately twenty times lower, two scenarios are possible. In the first scenario, sequential compression may occur (Fig. 8B_2), the total displacement of the flat plane consists of an initial compression of 250 μm (as determined by Hertzian analysis), during which the flat plane contacts solely with the fungiform papillae, followed by an additional indentation of about 100 μm with both fungiform and filiform papillae, in which the deformation of the filiform papillae was estimated by Hencky strain. Alternatively, if the flat plane rests solely on the filiform papillae, the indentation is about 120 μm (Fig. 8B_1). In both cases, the estimated thickness of two layers exceeds the largest size of WPM tested in this study. This calculation suggests that WPM at the lower layer may not contribute to lubrication through direct interaction with tribopair or the base surface of biomimetic tongue. However, particle accumulation in the lower layer may diminish hydrostatic pressure by reducing the papillated substrate's lubricant storage capacity, thereby lowering the hydrostatic lubrication efficiency compared with condition where no particles are present (Wu et al., 2021; Zou et al., 2022).

The thickness of the upper layer exceeding the dimension of WPM suggests that the WPM are expected to feed into the contact region in the lateral direction as the geometry forces them proceeding towards and eventually deforms the papillae completely, eventually flattening them *i.e.* crushing the papillae. During this process, WPM are expected to indent the papillae surface and disrupt the aqueous lubrication film, mirroring the results observed in smooth contact. Notable, the papillae indentation decreases with buildup of hydrodynamic lift force, therefore, the severest ball-papillae interaction is likely to occur in the lowest $U\eta_\infty$ value regime. This explains the observed higher friction coefficients in the lower $U\eta_\infty$ values regimes. As the $U\eta_\infty$ values increase, the thickness of the upper layer decreases with the buildup of hydrodynamic lift force, the upper geometry (ball)-papillae collisions are gradually diminished, accompanied with WPM exclusion, thereby explaining the convergence of friction behavior toward that of the buffer in the hydrodynamic regime (Fig. 7A–D).

Furthermore, the delubrication effect of WPM exhibited certain size dependence (Fig. 9 A and 9a). Given that the indentations are more than two orders of magnitude higher than the *hard* WPM-1 μm particles, these smaller particles demonstrate the most effective lubrication reduction, followed by *hard* WPM-10 μm and WPM-50 μm particles, whose dimensions are closer to the scales of indentation. Fig. 10 schematically illustrates this relationship, explaining the delubrication effect attributed to the ball-papillae collisions induced WPM entrapment.

Interestingly, *soft* WPM, which demonstrate superior lubrication performance in a smooth contact (Fig. 4D), did not exhibit any lubrication enhancement when tested under biomimetic surface (Fig. 7D). In fact, these particles increase friction before transitioning into the mixed regime, similar to their harder counterparts (see Fig. 9 B and 9b). The underlying reason for this observation is still unclear but may be related to the particle irregularities. Particles with sharper edges normally result in higher friction than spherical ones (De Wijk et al., 2005). Moreover, under a smooth contact, the large compliant contact region (apparent contact area is 14.65 mm^2, as estimated by Hertzian contact theory) would experience a much lower contact pressure. In a biomimetic tongue-like setup, WPM confined within a small compliant contact area (2.85 mm^2) are expected to suffer substantial higher contact pressure at the ball-papillae interface, which might facilitate particle penetration and disrupt boundary aqueous lubrication even with the *soft* WPM.

4. Limitations of the study

This study has three key limitations in the discussion of lubrication and delubricaiton mechanism of WPM dispersions. First, the current analyses of the apparent contact area and the indentation depths between the papillae and the glass probe were based on the assumption that both contact, and deformation occur perfectly in the vertical direction and in compliance with the Hertzian theory (i.e. indentation depth $\propto$ (load)$^{2/3}$, consequently, potential wobbling or bending of the papillae during collisions with the probe have not been considered. Such effects could significantly impact the actual contact area and the dynamics of papillae deformation. The authors do understand that alternative analytical approaches, such as finite element analysis, are urgently needed to capture these dynamic scenarios, however, this is beyond the scope of the present investigation. Second, the elastic modulus of the whey protein hydrogel was measured using oscillatory shear rheology, however, heating a small sample in the rheometer yields

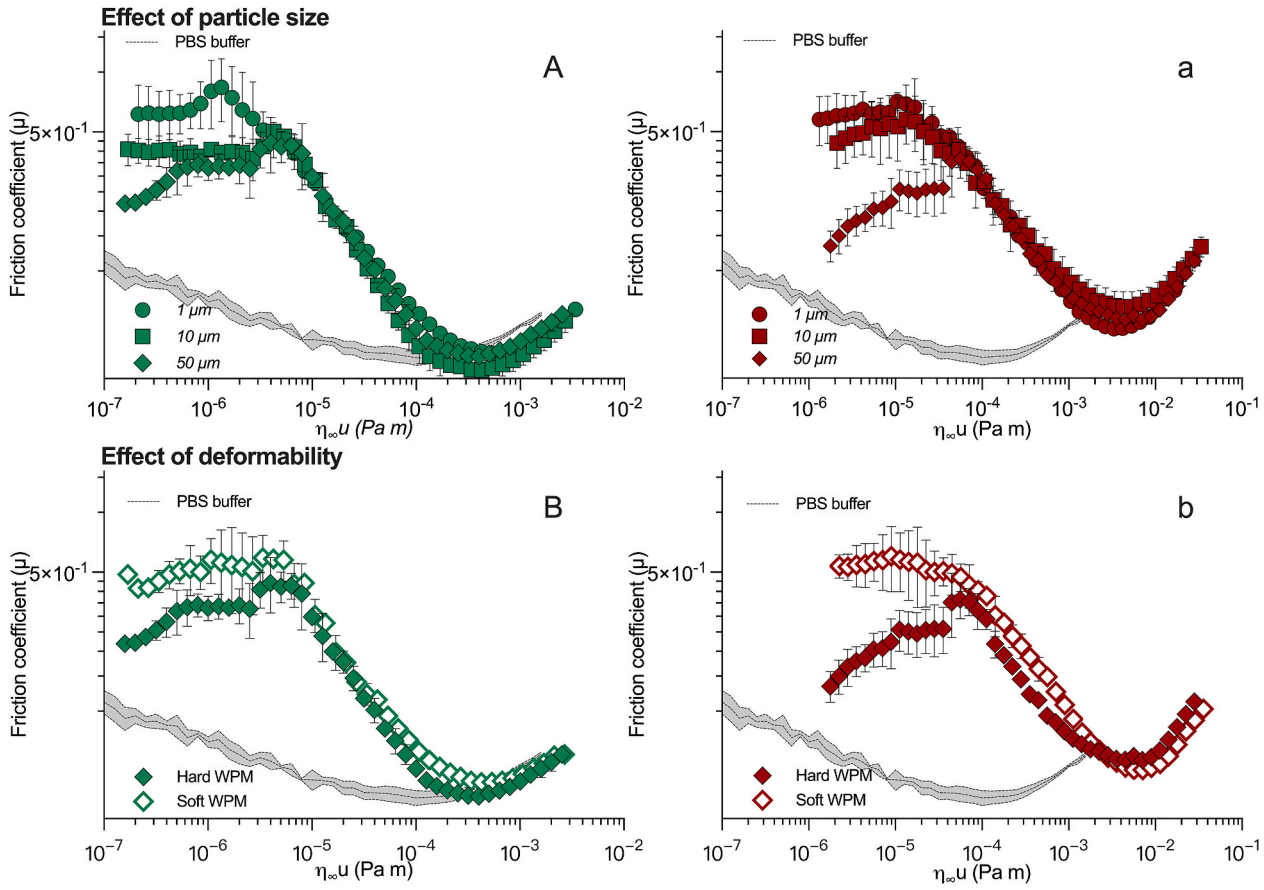

Fig. 9. Stribeck curves of WPM dispersions under ball-on-biomimetic tongue configurations. Friction curves of WPM with varied particle sizes (1, 10, and 50 μm) at volume fractions of 3 vol % (A) and 48 vol % (a). Stribeck curves of WPM with varied elastic modulus (85 kPa versus 350 kPa) at volume fractions of 3 vol % (B) and 48 vol % (b). Friction coefficients are plotted against a combined factor of the entrainment speed and the infinite plateau viscosity (η_∞). Phosphate buffer saline (PBS) is shown as control. Data are plotted as means and standard deviation shown as error bars of triplicate samples (n = 3 × 1).

gelation properties that may differ from those obtained for a macro-scale hydrogel formation within a beaker in a water bath. Thus, the actual difference in elastic modulus between the *hard* WPM and the elastomer may be substantially greater than the fourfold difference currently reported. Although particle interpenetration into the elastomer is a reasonable hypothesis from a mechanical perspective, further studies are needed employing techniques such as atomic force microscopy or surface force apparatus to accurately characterise microgel-substrate interactions at a single asperity contact.

The tongue surface is inherently weakly polar, but saliva coating renders it hydrophilic. This wettability shift closely reflects the cases presented in this study. However, our *in vitro* model does not capture saliva's intrinsic viscoelastic properties. *In vivo*, the salivary film behaves as a yield-stress fluid, sustaining load and maintaining film thickness under shear, which might mitigate the delubrication effects we observed in this study. To validate these hypotheses, sensory trials and tribological studies using real human saliva, and employing food-grade microgels are necessary undertakings.

5. Conclusions

This study demonstrates that tribological performance of micron-sized microgel-based lubricants is governed not only by the particles' physical attributes (*e.g.*, size and deformability) but also by the material properties of the contacting surfaces (smooth surface *versus* textured tongue-like surface). Ball-on-smooth disc friction measurements demonstrated that entrainment of relatively non-deformable particles was governed largely by the size ratio between the particles and the lubricant film thickness, latter generated by the hydrodynamic lift forces. The inclusion of *hard* WPM into a soft contact of similar wettability to that of human tongue exhibits a detrimental role in lubrication, with higher volume fraction of *hard* microgels causing increased friction coefficients. This is likely attributable to particle-induced indentation of the soft surface creating asperities that hinder the formation of effective hydration lubrication film. Conversely, *soft* WPM display superior lubricity in ball-on-smooth disc setup, possibly due to microgel deformation and entrainment into the contact. The oral-mimetic tribo-system, however, is more sensitive to the presence of WPM in the contact region, with a delubrication effect observed even at the lowest volume fractions, irrespective of the size and deformability of WPM. This behavior stems from the unique interfacial architecture between the spherical probe and papillae, which creates discrete lubricant reservoir that accommodate and interlocks the WPM and restricts mobility of the contact surfaces, increasing the frictional dissipation. Although sensory validation is lacking, the unique lubrication and delubrication behavior observed here for the first time may inspire rethinking of strategies for food, drug and oral care products development, when incorporating rigid micron-sized microgels particles that require interacting with texturized, soft bio-surfaces such as human tongue.

CRediT authorship contribution statement

Qi Wang: Writing – review & editing, Writing – original draft, Visualization, Project administration, Methodology, Investigation, Funding acquisition, Formal analysis, Data curation, Conceptualization. **Siavash Soltanahmadi:** Writing – review & editing, Supervision,

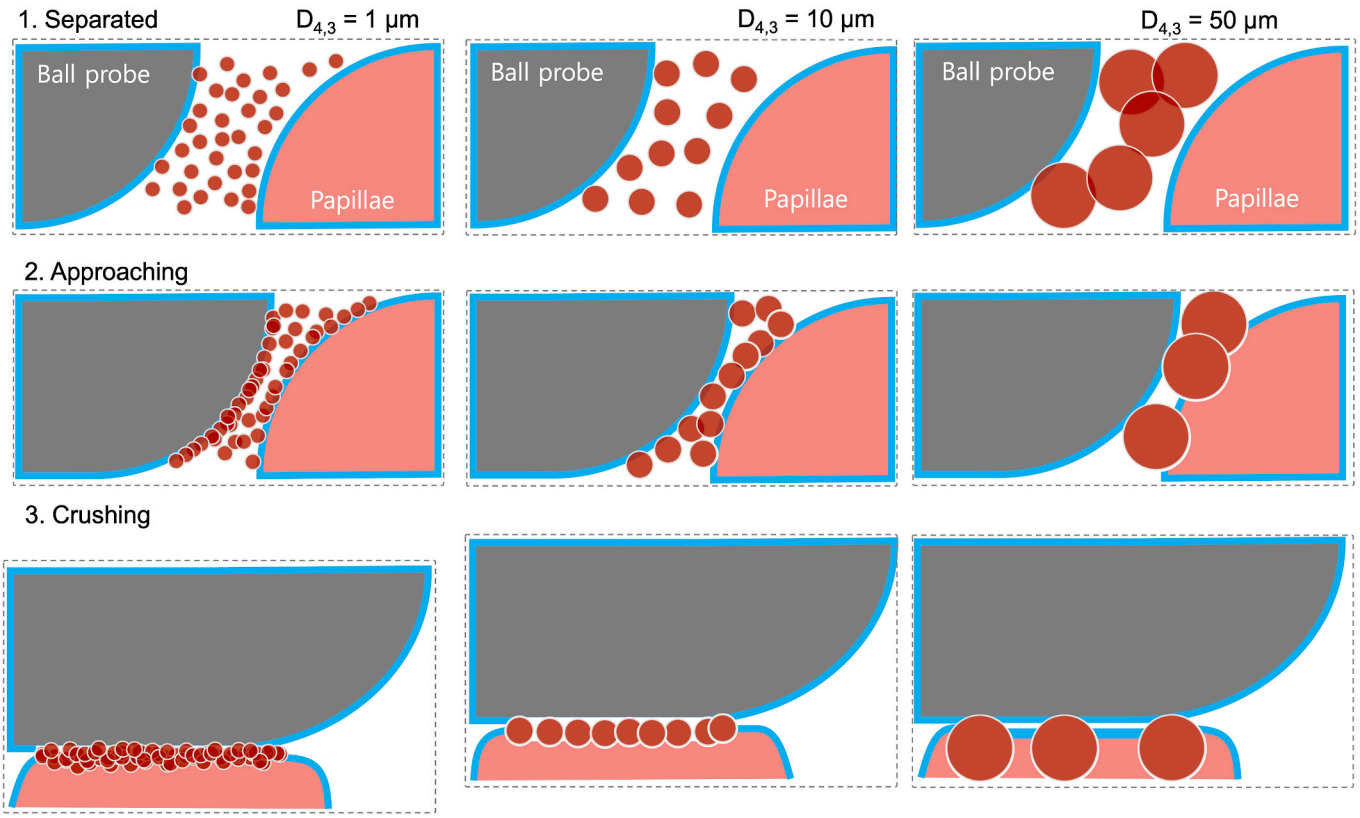

Fig. 10. Schematic illustration of the delubrication effect of *hard* WPM, highlighting three phases of upper geometry (ball)-papillae interaction. (1) Separation Phase: The geometry and papillae disengage, leaving WPM sparsely distributed in the upper layer. (2) Approach Phase: As the upper surface moves closer, WPM jam and assemble at the interface between the upper surface and the papillae surfaces. (3) Smashing Phase: Upon impact, the upper surfaces deform the papillae, allowing WPM to interpenetrate the papillae surface. The thickness of the upper layer is two orders of magnitude greater than the size of *hard* WPM-1 μm particles, facilitating their inclusion in the lateral contact between the geometry and papillae. In contrast, the indentation of the papillae is of a similar order to the sizes of *hard* WPM-10 μm and *hard* WPM-50 μm particles, which impedes their presence in the contact region.

Methodology, Conceptualization. **Jianshe Chen:** Writing – review & editing, Supervision. **Anwesha Sarkar:** Writing – review & editing, Supervision, Project administration, Methodology, Conceptualization.

Declaration of competing interest

None.

Acknowledgments

Author Qi Wang would like to thank China Scholarship Council (No. 202308330506) for funding his visit and carrying out this work at the University of Leeds, UK.

Appendix A. Supplementary data

Supplementary data to this article can be found online at https://doi.org/10.1016/j.foodhyd.2025.111908.

Data availability

Data will be made available on request.

References

Akgonullu, D. Z., Murray, B. S., Connell, S. D., Fang, Y., Linter, B., & Sarkar, A. (2023). Synthetic and biopolymeric microgels: Review of similarities and difference in behaviour in bulk phases and at interfaces. *Advances in Colloid and Interface Science, 320*, Article 102983.

Akgonullu, D. Z., O'Hagan, N. M., Murray, B. S., Connell, S. D., Fang, Y., Linter, B. R., & Sarkar, A. (2024). Bulk and interfacial behavior of potato protein-based microgels. *Langmuir, 40*(41), 21341–21351.

Andablo-Reyes, E., Bryant, M., Neville, A., Hyde, P., Sarkar, R., Francis, M., & Sarkar, A. (2020). 3D biomimetic tongue-emulating surfaces for tribological applications. *ACS Applied Materials & Interfaces, 12*(44), 49371–49385.

Andablo-Reyes, E., Yerani, D., Fu, M., Liamas, E., Connell, S., Torres, O., & Sarkar, A. (2019). Microgels as viscosity modifiers influence lubrication performance of continuum. *Soft Matter, 15*(47), 9614–9624.

Beldengrün, Y., Aragon, J., Prazeres, S. F., Montalvo, G., Miras, J., & Esquena, J. (2018). Gelatin/maltodextrin water-in-water (W/W) emulsions for the preparation of cross-linked enzyme-loaded microgels. *Langmuir, 34*(33), 9731–9743.

Bhushan, B. (2013). Fluid film lubrication. In *Introduction to tribology* (pp. 399–500). United Kingdom: Wiley. Chicheste, West Sussex.

Blau, P. J. (2005). On the nature of running-in. *Tribology International, 38*(11), 1007–1012.

Bongaerts, J. H. H., Fourtouni, K., & Stokes, J. R. (2007). Soft-tribology: Lubrication in a compliant PDMS–PDMS contact. *Tribology International, 40*(10), 1531–1542.

Brenner, H. (1974). Rheology of a dilute suspension of axisymmetric Brownian particles. *International Journal of Multiphase Flow, 1*(2), 195–341.

Brown, E., Zhang, H., Forman, N. A., Maynor, B. W., Betts, D. E., DeSimone, J. M., & Jaeger, H. M. (2011). Shear thickening and jamming in densely packed suspensions of different particle shapes. *Physical Review E, 84*(3), Article 031408.

Çakır, E., & Foegeding, E. A. (2011). Combining protein micro-phase separation and protein–polysaccharide segregative phase separation to produce gel structures. *Food Hydrocolloids, 25*(6), 1538–1546.

Chen, J., & Stokes, J. R. (2012). Rheology and tribology: Two distinctive regimes of food texture sensation. *Trends in Food Science & Technology, 25*(1), 4–12.

Chernyak, Y. B., & Leonov, A. I. (1986). On the theory of the adhesive friction of elastomers. *Wear, 108*(2), 105–138.

Chojnicka-Paszun, A., Doussinault, S., & de Jongh, H. H. J. (2014). Sensorial analysis of polysaccharide–gelled protein particle dispersions in relation to lubrication and viscosity properties. *Food Research International, 56*, 199–210.

Chu, Y., Jo, Y., & Chen, L. (2022). Size-controllable core/shell whey protein microgels with narrow particle size distribution fabricated by a facile method. *Food Hydrocolloids, 124*, Article 107316.

Chu, Y., Zhao, Z., Schreiber, S., Zeng, H., & Chen, L. (2024). Size-controllable and pH-sensitive whey protein microgels as high-performance aqueous biolubricants. *ACS Applied Materials & Interfaces, 16*(35), 46909–46922.
de Vicente, J., Stokes, J. R., & Spikes, H. A. (2005). The frictional properties of Newtonian fluids in rolling - Sliding soft-EHL contact. *Tribology Letters, 20*(3–4), 273–286.
de Wijk, R. A., & Prinz, J. F. (2005). The role of friction in perceived oral texture. *Food Quality and Preference, 16*(2), 121–129.
de Wijk, R. A., Prinz, J. F., & Janssen, A. M. (2006). Explaining perceived oral texture of starch-based custard desserts from standard and novel instrumental tests. *Food Hydrocolloids, 20*(1), 24–34.
Farjami, T., & Madadlou, A. (2017). Fabrication methods of biopolymeric microgels and microgel-based hydrogels. *Food Hydrocolloids, 62*, 262–272.
Gabriele, A., Spyropoulos, F., & Norton, I. T. (2010). A conceptual model for fluid gel lubrication. *Soft Matter, 6*(17), 4205–4213.
Garrec, D. A., & Norton, I. T. (2012). Boundary lubrication by sodium salts: A Hofmeister series effect. *Journal of Colloid and Interface Science, 379*(1), 33–40.
Garrec, D. A., & Norton, I. T. (2013). Kappa carrageenan fluid gel material properties. Part 2: Tribology. *Food Hydrocolloids, 33*(1), 160–167.
Genovese, D. B. (2012). Shear rheology of hard-sphere, dispersed, and aggregated suspensions, and filler-matrix composites. *Advances in Colloid and Interface Science, 171–172*, 1–16.
GonzÁLez-Tello, P., Camacho, F., Guadix, E. M., LuzÓN, G., & GonzÁLez, P. A. (2009). Density, viscosity and surface tension of whey protein concentrate solutions. *Journal of Food Process Engineering, 32*(2), 235–247.
Hamrock, B. J., & Dowson, D. (1977). Isothermal elastohydrodynamic lubrication of point contacts: Part III—Fully flooded results. *Journal of Lubrication Technology, 99*(2), 264–275.
Highley, C. B., Song, K. H., Daly, A. C., & Burdick, J. A. (2019). Jammed microgel inks for 3D printing applications. *Advanced Science, 6*(1), Article 1801076.
Hirano, F., & Yamamoto, S. (1959). Four-ball test on lubricating oils containing solid particles. *Wear, 2*(5), 349–363.
Hu, J., Andablo-Reyes, E., Soltanahmadi, S., & Sarkar, A. (2020). Synergistic microgel-reinforced hydrogels as high-performance lubricants. *ACS Macro Letters, 9*(12), 1726–1731.
Imai, E., Saito, K., Hatakeyama, M., Hatae, K., & Shimada, A. (1999). Effect of physical properties of food particles on the degree of graininess perceived in the mouth. *Journal of Texture Studies, 30*(1), 59–88.
Kew, B., Holmes, M., Liamas, E., Ettelaie, R., Connell, S. D., Dini, D., & Sarkar, A. (2023). Transforming sustainable plant proteins into high performance lubricating microgels. *Nature Communications, 14*(1), 4743.
Kullaa, A., Sorvari, T. E., Kullaa-Mikkonen, A., & Sorvari, T. E. (1985). A scanning electron microscopic study of the dorsal surface of the human tongue. *Cells Tissues Organs, 123*(2), 114–120.
Liu, K., Stieger, M., van der Linden, E., & van de Velde, F. (2016). Effect of microparticulated whey protein on sensory properties of liquid and semi-solid model foods. *Food Hydrocolloids, 60*, 186–198.
Lobry, L., Lemaire, E., Blanc, F., Gallier, S., & Peters, F. (2019). Shear thinning in Non-Brownian suspensions explained by variable friction between particles. *Journal of Fluid Mechanics, 860*, 682–710.
Moayedi, Y., Duenas-Bianchi, L. F., & Lumpkin, E. A. (2018). Somatosensory innervation of the oral mucosa of adult and aging mice. *Scientific Reports, 8*(1), 1–14.
Moayedi, Y., Michlig, S., Park, M., Koch, A., & Lumpkin, E. A. (2021). Somatosensory innervation of healthy human oral tissues. *Journal of Comparative Neurology, 529*(11), 3046–3061.
Murray, B. S. (2019). Microgels at fluid-fluid interfaces for food and drinks. *Advances in Colloid and Interface Science, 271*, Article 101990.
Myant, C., Spikes, H. A., & Stokes, J. R. (2010). Influence of load and elastic properties on the rolling and sliding friction of lubricated compliant contacts. *Tribology International, 43*(1–2), 55–63.
Myshkin, N. K., Petrokovets, M. I., & Kovalev, A. V. (2005). Tribology of polymers: Adhesion, friction, wear, and mass-transfer. *Tribology International, 38*(11), 910–921.
Nicolai, T. (2016). Formation and functionality of self-assembled whey protein microgels. *Colloids and Surfaces B: Biointerfaces, 137*, 32–38.
Nicolai, T., & Durand, D. (2013). Controlled food protein aggregation for new functionality. *Current Opinion in Colloid & Interface Science, 18*(4), 249–256.
Nikolov, S. V., Fernandez-Nieves, A., & Alexeev, A. (2020). Behavior and mechanics of dense microgel suspensions. *Proceedings of the National Academy of Sciences, 117*(44), 27096–27103.
Papadopoulou, A., Gillissen, J. J., Wilson, H. J., Tiwari, M. K., & Balabani, S. (2020). On the shear thinning of Non-Brownian suspensions: Friction or adhesion? *Journal of Non-Newtonian Fluid Mechanics, 281*, Article 104298.
Peng, Y., Serfass, C. M., Kawazoe, A., Shao, Y., Gutierrez, K., Hill, C. N., Santos, V. J., Visell, Y., & Hsiao, L. C. (2021). Elastohydrodynamic friction of robotic and human fingers on soft micropatterned substrates. *Nature Materials, 20*(12), 1707–1711.
Ranc, H., Servais, C., Chauvy, P. F., Debaud, S., & Mischler, S. (2006). Effect of surface structure on frictional behaviour of a tongue/palate tribological system. *Tribology International, 39*(12), 1518–1526.
Raviv, U., & Klein, J. (2002). Fluidity of bound hydration layers. *Science, 297*(5586), 1540–1543.
Rudge, R. E. D., Mosselman, M. J., Shewan, H. M., Stokes, J. R., Dijksman, J. A., & Scholten, E. (2023). The impact of tribometer motion and surface roughness on the frictional regimes of model foods. *Food Hydrocolloids, 145*, Article 108976.
Rudge, R. E. D., Shewan, H. M., Stokes, J. R., Dijksman, J. A., & Scholten, E. (2025). Dynamics of particle entrainment for glass particles suspended in various fluids. *Tribology International, 202*, Article 110235.
Rudge, R. E. D., van de Sande, J. P. M., Dijksman, J. A., & Scholten, E. (2020). Uncovering friction dynamics using hydrogel particles as soft ball bearings. *Soft Matter, 16*(15), 3821–3831.
Sağlam, D., Venema, P., de Vries, R., Sagis, L. M. C., & van der Linden, E. (2011). Preparation of high protein micro-particles using two-step emulsification. *Food Hydrocolloids, 25*(5), 1139–1148.
Sarkar, A., Andablo-Reyes, E., Bryant, M., Dowson, D., & Neville, A. (2019). Lubrication of soft oral surfaces. *Current Opinion in Colloid & Interface Science, 39*, 61–75.
Sarkar, A., & Dickinson, E. (2020). Sustainable food-grade Pickering emulsions stabilized by plant-based particles. *Current Opinion in Colloid & Interface Science, 49*, 69–81.
Sarkar, A., Kanti, F., Gulotta, A., Murray, B. S., & Zhang, S. (2017). Aqueous lubrication, structure and rheological properties of whey protein microgel particles. *Langmuir, 33*(51), 14699–14708.
Sarkar, A., Soltanahmadi, S., Chen, J., & Stokes, J. R. (2021). Oral tribology: Providing insight into oral processing of food colloids. *Food Hydrocolloids, 117*, 106635-106635.
Selway, N., Chan, V., & Stokes, J. (2017). Influence of fluid viscosity and wetting on multiscale viscoelastic lubrication in soft tribological contacts. *Soft Matter, 13*.
Shewan, H. M., Stokes, J. R., & Smyth, H. E. (2020). Influence of particle modulus (softness) and matrix rheology on the sensory experience of 'grittiness' and 'smoothness'. *Food Hydrocolloids, 103*, Article 105662.
Sivakumaran, D., Maitland, D., & Hoare, T. (2011). Injectable microgel-hydrogel composites for prolonged small-molecule drug delivery. *Biomacromolecules, 12*(11), 4112–4120.
Soltanahmadi, S., Bryant, M., & Sarkar, A. (2023). Insights into the multiscale lubrication mechanism of edible phase change materials. *ACS Applied Materials & Interfaces, 15*(3), 3699–3712.
Soltanahmadi, S., Murray, B. S., & Sarkar, A. (2022). Comparison of oral tribological performance of proteinaceous microgel systems with protein-polysaccharide combinations. *Food Hydrocolloids, 129*, Article 107660.
Spikes, H. (2015). Basics of EHL for practical application. *Lubrication Science, 27*(1), 45–67.
Stickel, J. J., & Powell, R. L. (2005). Fluid mechanics and rheology of dense suspensions. *Annual Review of Fluid Mechanics, 37*, 129–149.
Stokes, J. R., Boehm, M. W., & Baier, S. K. (2013). Oral processing, texture and mouthfeel: From rheology to tribology and beyond. *Current Opinion in Colloid & Interface Science, 18*(4), 349–359.
Taylor, B. L., & Mills, T. B. (2020). Surface texture modifications for oral processing applications. *Biotribology, 23*, 100132-100132.
Tenorio-Garcia, E., Rappolt, M., Sadeghpour, A., Simone, E., & Sarkar, A. (2024). Fabrication and stability of dual Pickering double emulsions stabilized with food-grade particles. *Food Hydrocolloids, 156*, Article 110327.
Torres, O., Andablo-Reyes, E., Murray, B. S., & Sarkar, A. (2018). Emulsion microgel particles as high-performance bio-lubricants. *ACS Applied Materials & Interfaces, 10*(32), 26893–26905.
Verheul, M., & Roefs, S. P. F. M. (1998). Structure of particulate whey protein gels: Effect of NaCl concentration, pH, heating temperature, and protein composition. *Journal of Agricultural and Food Chemistry, 46*(12), 4909–4916.
Wang, X., Chen, J., & Wang, X. (2022). In situ oral lubrication and smoothness sensory perception influenced by tongue surface roughness. *Journal of the Science of Food and Agriculture, 102*(1), 132–138.
Wang, Q., Zhu, Y., & Chen, J. (2021). Development of a simulated tongue substrate for in vitro soft "oral" tribology study. *Food Hydrocolloids, 120*, Article 106991.
Wu, Z., Bao, H., Xing, Y., & Liu, L. (2021). Tribological characteristics and advanced processing methods of textured surfaces: A review. *The International Journal of Advanced Manufacturing Technology, 114*(5), 1241–1277.
Wu, H., Qin, L., Dong, G., Hua, M., Yang, S., & Zhang, J. (2017). An investigation on the lubrication mechanism of MoS2 nano sheet in point contact: The manner of particle entering the contact area. *Tribology International, 107*, 48–55.
Wu, H., Qin, L., Zeng, Q., & Dong, G. (2015). Understanding the physical adsorption action mechanism of MoS2 nanoparticles in boundary lubrication with different polyisobutyleneamine succinimide (PIBS) concentrations. *Tribology Letters, 60*(2), 26.
Xu, Y., Cartwright, B., Advincula, L., Myant, C., & Stokes, J. R. (2021). Generalised scaling law for soft contact tribology: Influence of load and asymmetric surface deformation. *Tribology International, 163*, Article 107192.
Yakubov, G. E., Branfield, T. E., Bongaerts, J. H. H. H., & Stokes, J. R. (2015). Tribology of particle suspensions in rolling-sliding soft contacts. *Biotribology, 3*, 1–10.
You, K.-M., Murray, B. S., Connell, S. D., & Sarkar, A. (2024). Fabrication and lubrication performance of sustainable pickering-like water-in-water emulsions using plant protein microgels. *Nano Select, 5*(4), Article 2300160.
Zou, H., Lin, B., Ren, X., Li, H., Diao, Q., Wang, Y., Sui, T., & Yan, S. (2022). Particle size effects on efficiency of surface texturing in reducing friction. *Tribology International, 176*, Article 107895.